

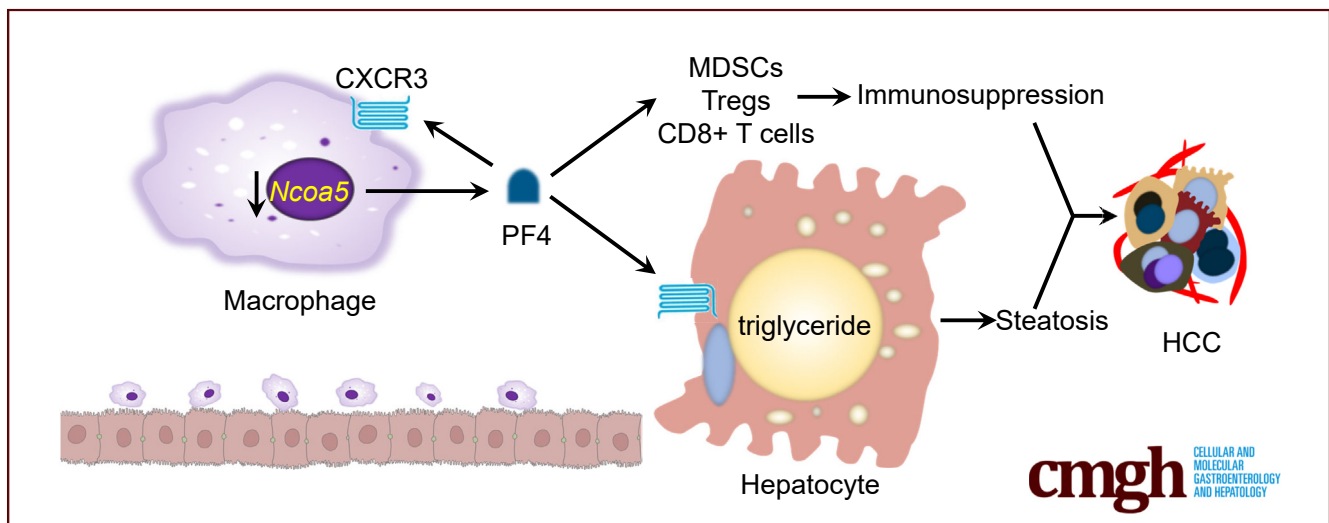
ORIGINAL RESEARCH

NCOA5 Haploinsufficiency in Myeloid-Lineage Cells Sufficiently Causes Nonalcoholic Steatohepatitis and Hepatocellular Carcinoma



Yueqi Zhang,^{1,2} Yue Luo,^{2,3,4} Xinhui Liu,^{2,3,4} Matti Kiupel,⁵ Aimin Li,^{3,4} Hongbing Wang,² Qing-Sheng Mi,^{6,7} and Hua Xiao²

¹Cell and Molecular Biology Program, Michigan State University, East Lansing, Michigan; ²Department of Physiology, Michigan State University, East Lansing, Michigan; ³Cancer Center, Southern Medical University, Guangzhou, Guangdong, China; ⁴Integrated Hospital of Traditional Chinese Medicine, Southern Medical University, Guangzhou, Guangdong, China; ⁵Department of Pathobiology and Diagnostic Investigation, Michigan State University, East Lansing, Michigan; ⁶Immunology Program, Henry Ford Cancer Institute, Henry Ford Health, Detroit, Michigan; and ⁷Center for Cutaneous Biology and Immunology, Department of Dermatology, Henry Ford Health, Detroit, Michigan



SUMMARY

NCOA5 haploinsufficiency in myeloid-lineage cells sufficiently causes NASH and HCC in male mice partially through up-regulated macrophage PF4. The transcriptome of NCOA5 haploinsufficient intrahepatic macrophages resembles that of obese and NAFLD humans, and the high PF4 expression correlated with poor prognosis of HCC patients.

BACKGROUND & AIMS: The nuclear receptor coactivator 5 (NCOA5) is a putative type 2 diabetes susceptibility gene. NCOA5 haploinsufficiency results in the spontaneous development of nonalcoholic fatty liver disease (NAFLD), insulin resistance, and hepatocellular carcinoma (HCC) in male mice; however, the cell-specific effect of NCOA5 haploinsufficiency in various types of cells, including macrophages, on the development of NAFLD and HCC remains unknown.

METHODS: Control and myeloid-lineage-specific *Ncoa5* deletion (*Ncoa5*^{ΔM/+}) mice fed a normal diet were examined for the development of NAFLD, nonalcoholic steatohepatitis (NASH),

and HCC. Altered genes and signaling pathways in the intrahepatic macrophages of *Ncoa5*^{ΔM/+} male mice were analyzed and compared with those of obese human individuals. The role of platelet factor 4 (PF4) in macrophages and the underlying mechanism by which PF4 affects NAFLD/NASH were explored in vitro and in vivo. PF4 expression in HCC patient specimens and prognosis was examined.

RESULTS: Myeloid-lineage-specific *Ncoa5* deletion sufficiently causes spontaneous NASH and HCC development in male mice fed a normal diet. PF4 overexpression in *Ncoa5*^{ΔM/+} intrahepatic macrophages is identified as a potent mediator to trigger lipid accumulation in hepatocytes by inducing lipogenesis-promoting gene expression. The transcriptome of intrahepatic macrophages from *Ncoa5*^{ΔM/+} male mice resembles that of obese human individuals. High PF4 expression correlated with poor prognosis of HCC patients and increased infiltrations of M2 macrophages, regulatory T cells, and myeloid-derived suppressor cells in HCCs.

CONCLUSIONS: Our findings reveal a novel mechanism for the onset of NAFLD/NASH and HCC initiated by NCOA5-deficient macrophages, suggesting the NCOA5-PF4 axis in macrophages

as a potential target for developing preventive and therapeutic interventions against NAFLD/NASH and HCC. (*Cell Mol Gastroenterol Hepatol* 2024;17:1–27; <https://doi.org/10.1016/j.jcmgh.2023.09.007>)

Keywords: NAFLD; NASH; HCC; PF4.

Nonalcoholic fatty liver disease (NAFLD), consisting of nonalcoholic fatty liver, also known as hepatic steatosis, and nonalcoholic steatohepatitis (NASH), affects approximately 25% of the world population.¹ Patients commonly develop NAFLD because of susceptible genetic and environmental factors, a substantial proportion of which progress to NASH. Some eventually advance to cirrhosis and hepatocellular carcinoma (HCC).² Cumulating evidence suggests that multiple parallel factors, including dietary factors, hormones, and gut microbiota, act together on genetically predisposed individuals, promoting the development of insulin resistance, endoplasmic reticulum stress, mitochondrial dysfunction, and release of proinflammatory cytokines, thereby inducing NAFLD and NASH.³ Human and animal studies have provided convincing data suggesting that intrahepatic resident macrophages and recruited macrophages play a crucial role in the pathogenesis of NAFLD/NASH and HCC via promoting chronic inflammation, lipogenesis, and the formation of an immunosuppressive microenvironment.⁴ In response to extrinsic signals from the microenvironment, the intrahepatic macrophages were found to polarize toward a proinflammatory phenotype and release proinflammatory cytokines, nitric oxide, and reactive oxygen species in the liver, leading to the recruitment of other immune cells such as B and T cells, DNA damage, and cell death of hepatocytes. The combination of these alterations in the liver results in chronic inflammation, hepatic fibrosis, and immunosuppression, eventually advancing to HCC. However, how distinct cellular factors and signal pathways that intrinsically regulate the polarization and functions of heterogeneous macrophages contribute to the pathogenesis of these diseases is incompletely understood. Moreover, whether genetic and epigenetic risk factors in macrophages can sufficiently cause the development of NAFLD and HCC remains unknown.

Nuclear receptor coactivator 5 (NCOA5) is a unique coactivator for several known nuclear receptors, including estrogen receptor α and liver X receptor, having both transcriptional coactivator and corepressor activities.^{5–7} Analysis of single nucleotide polymorphisms in chromosome 20q12-13.1 region for associations with type 2 diabetes (T2D) and body mass index in European American case-control populations revealed that the *NCOA5* is a T2D susceptibility gene candidate.⁸ We previously reported that heterozygous deletion of the *Ncoa5* resulted in the development of hepatic steatosis, insulin resistance, and HCC in mice in a male-biased manner. The development of these diseases was accompanied by increased infiltrating immune cells, including macrophages, and overexpressed proinflammatory cytokines in the liver.^{9,10} Although these observations indicate the importance of NCOA5 in suppressing

hepatocarcinogenesis, it remains to be understood how NCOA5 regulates the development of hepatic steatosis and HCC, especially in macrophages. Here we demonstrate that NCOA5 in intrahepatic macrophages plays a crucial role in regulating the interaction of macrophages with hepatocytes. Its haploinsufficiency in myeloid-lineage cells sufficiently induced the development of NAFLD/NASH and HCC in male mice, at least partially, through overexpression of platelet factor 4 (PF4) in intrahepatic macrophages.


Results

Myeloid-Lineage-Specific Heterozygous Deletion of Ncoa5 Results in Spontaneous Metabolic Syndrome and HCC Development in Male Mice Fed a Normal Diet

To study the underlying mechanism and cell-specific impact of *Ncoa5* haploinsufficiency on NAFLD and HCC development, we generated C57BL/6 mice carrying the *Ncoa5* allele with loxP-flanked exons 3 and 4 (*Ncoa5*^{fl}), which are the identical targeted exons in *Ncoa5*^{+/-} mouse⁹ (Figure 1A). We were particularly interested in the role of NCOA5 in regulating macrophage function. *Ncoa5*^{ΔM/+} (*Ncoa5*^{fl/+}/LysM^{cre/+}) mice were generated by crossing *Ncoa5*^{fl/fl} mice with LysM^{cre} mice (Jackson Lab) that allow for cre-mediated deletion in myeloid-lineage cells, including mature macrophages, some neutrophils and monocytes, and few dendritic cells.¹¹ Deletion of the *Ncoa5* gene in intrahepatic macrophages was confirmed by Western blotting using *Ncoa5*^{ΔM/+} (*Ncoa5*^{fl/+}/LysM^{cre/+}) and *Ncoa5*^{ΔM/ΔM} (*Ncoa5*^{fl/fl}/LysM^{cre/+}) mice (Figure 1B and C). Mice with cre-mediated cell type-specific *Ncoa5* deletion in hepatocytes were also generated by crossing *Ncoa5*^{fl/fl} mice with *Speer6-ps1*^{Alb-cre/+} mice and confirmed by Western blotting (Figure 1D). *Ncoa5*^{ΔM/+}, *Ncoa5*^{ΔM/ΔM}, and *Ncoa5*^{ΔH/ΔH} mice were viable and fertile with normal litter size.

To circumvent the possible cell development defects associated with *Ncoa5* homozygous loss and better compare with the previous phenotypes in *Ncoa5*^{+/-} mice, we focused on *Ncoa5*^{ΔM/+} mice. We examined the fasting serum

Abbreviations used in this paper: ALT, alanine transaminase; AMLN, Amylin liver NASH; CM, conditioned medium; DEG, differently expressed gene; DMEM, Dulbecco modified Eagle medium; GAGE, generally applicable gene-set enrichment; GeRP, glucan-encapsulated siRNA particle; GSEA, gene set enrichment analysis; GTT, glucose tolerance test; HCC, hepatocellular carcinoma; IHC, immunohistochemistry; IL, interleukin; ITT, insulin tolerance test; KEGG, Kyoto encyclopedia of genes and genomes; LIHC, liver hepatocellular carcinoma; MDSCs, myeloid-derived suppressor cells; NAFLD, nonalcoholic fatty liver disease; NASH, nonalcoholic steatohepatitis; NCOA5, nuclear receptor coactivator 5; PF4, platelet factor 4; RNA-seq, RNA sequencing; RT-qPCR, real-time quantitative polymerase chain reaction; SEM, standard error of mean; siRNA, small interfering RNA; ssGSEA, single-sample gene set enrichment analysis; T2D, type 2 diabetes; TCGA, The Cancer Genome Atlas; TNF, tumor necrosis factor; TPM, transcripts per million; Tregs, regulatory T cells.

 Most current article

© 2023 The Authors. Published by Elsevier Inc. on behalf of the AGA Institute. This is an open access article under the CC BY-NC-ND license (<http://creativecommons.org/licenses/by-nc-nd/4.0/>).

2352-345X

<https://doi.org/10.1016/j.jcmgh.2023.09.007>

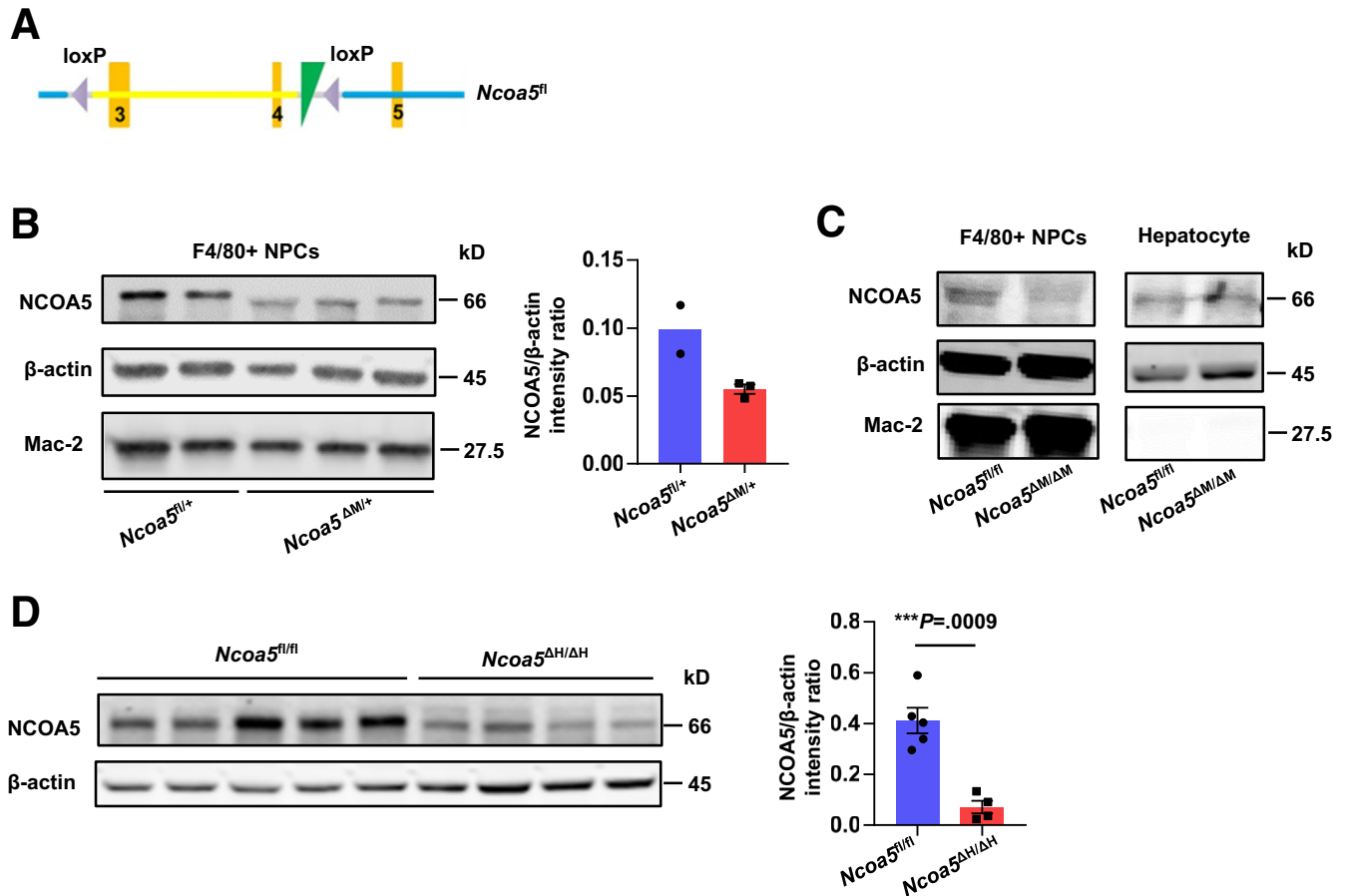


Figure 1. Validation of cell type–specific *Ncoa5* deletion in mice. (A) Schematic representation of the floxed *Ncoa5* gene. (B and C) Western blot analysis of myeloid-lineage–specific *Ncoa5* heterozygous deletion or knockout in *Ncoa5^{ΔM/+}* or *Ncoa5^{ΔM/ΔM}* males. Nonparenchymal cells (NPCs) and parenchymal cells (PCs, hepatocytes) were isolated from the mouse liver using a 2-step perfusion method. F4/80+ cells were isolated using Anti-F4/80 MicroBeads from NPCs. Error bar represents SEM. (D) Western blot validation of reduced NCOA5 expression in the liver lysate of *Ncoa5^{ΔH/ΔH}* males ($n = 4$) compared with *Ncoa5^{fl/fl}* males ($n = 5$). Data represent mean \pm SEM. Two-tailed unpaired *t* test. *** $P < .001$.

glucose, glucose tolerance, and insulin tolerance on 7- to 8-week-old *Ncoa5^{fl/+}* and *Ncoa5^{ΔM/+}* mice fed a normal diet. Although the fasting blood glucose level was comparable between the *Ncoa5^{ΔM/+}* and *Ncoa5^{fl/+}* male mice, the glucose tolerance and insulin sensitivity were significantly decreased in *Ncoa5^{ΔM/+}* male mice compared with *Ncoa5^{fl/+}* male mice (Figure 2A). There was no significant difference in glucose tolerance and insulin sensitivity between the 2 groups of female mice (Figure 2B). This result is consistent with the fact that no significant phenotypes were observed in *Ncoa5^{+/-}* female mice⁹; thus, we focus our studies on *Ncoa5^{ΔM/+}* male mice. At 5 months of age, *Ncoa5^{ΔM/+}* male mice had significantly increased body weight compared with *Ncoa5^{fl/+}* male mice (Figure 2C), and some *Ncoa5^{ΔM/+}* male mice had mild microvesicular steatosis (Figure 2D). Finally, spontaneous HCC was observed in *Ncoa5^{ΔM/+}* male mice starting at 10 months of age. Twenty-five percent of *Ncoa5^{ΔM/+}* male mice developed liver tumors. In contrast, no liver tumor was found in *Ncoa5^{fl/+}* male mice over 18 months (Figure 2E). The liver tumors in *Ncoa5^{ΔM/+}* male mice were well to moderately differentiated HCCs

associated with hepatic steatosis (Figure 2F). Altogether, these results suggest that myeloid-lineage–specific heterozygous deletion of *Ncoa5* is sufficient to induce the spontaneous development of the metabolic syndrome and a moderate incidence of HCC in mice in a male-biased manner.

Myeloid-Lineage–Specific Heterozygous Deletion of *Ncoa5* Results in the Spontaneous Development of NASH in Aged Male Mice Fed a Normal Diet

To evaluate the impact of myeloid-lineage–specific heterozygous deletion of *Ncoa5* on the liver at the preneoplastic step of hepatocarcinogenesis, we examined the postmortem livers of 10-month-old *Ncoa5^{fl/+}* and *Ncoa5^{ΔM/+}* mice. Most of the livers from *Ncoa5^{ΔM/+}* male mice have a much lighter color than control livers (Figure 3A). Seventy-three percent of *Ncoa5^{ΔM/+}* male mice exhibited moderate to severe steatosis because H&E staining showed moderate to marked centrilobular macrovesicular steatosis and was associated with mild to moderate inflammatory infiltrates in the liver

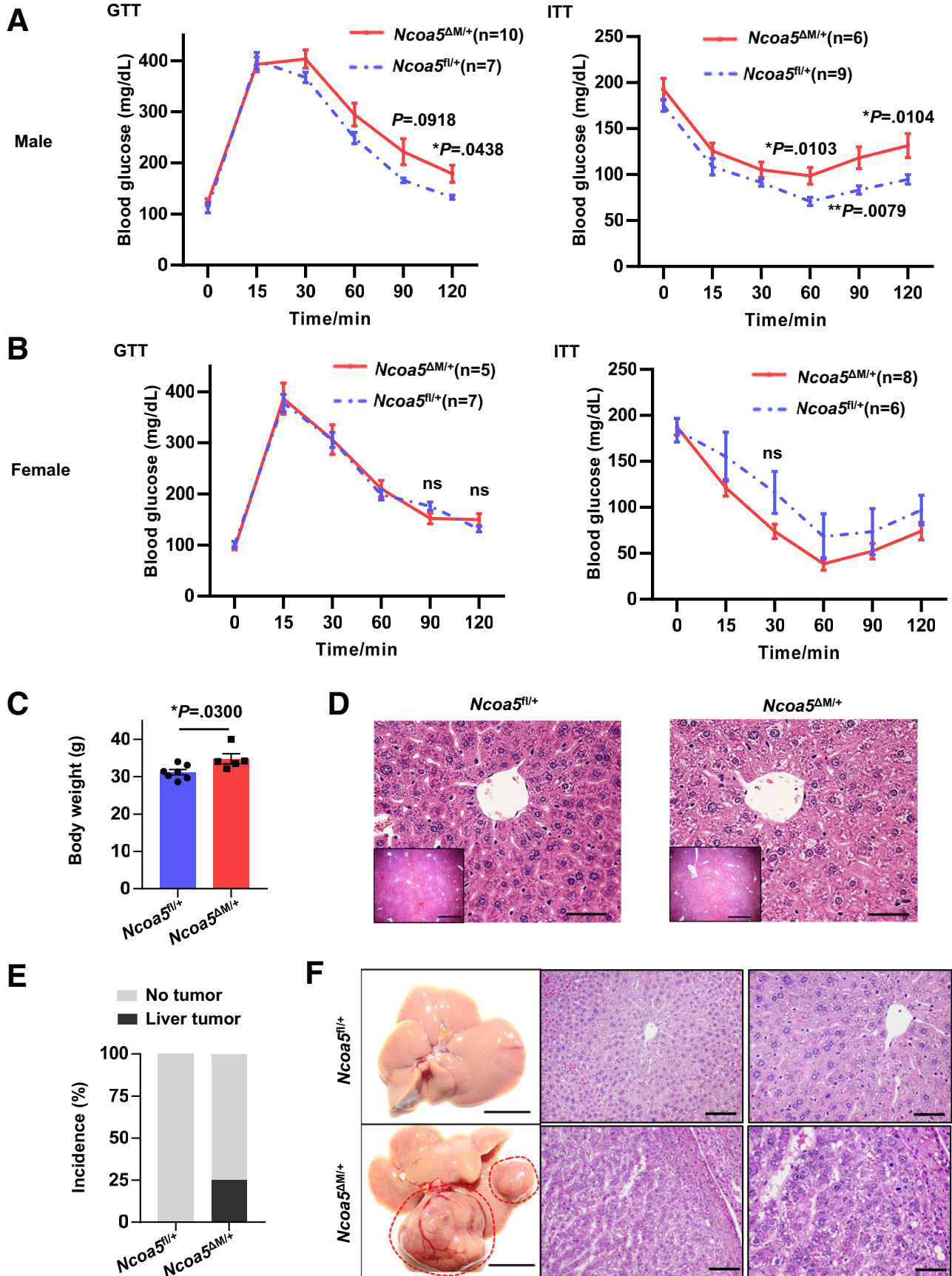


(Figure 3B and C). *Ncoa5*^{ΔM/+} male mice also had significantly increased body weight (Figure 3D). Markedly increased hepatic lipid content in these mice was detected by Oil-Red-O staining and measured with triglyceride colorimetric assay (Figure 3E and F). The number of macrophages significantly increased in the livers of *Ncoa5*^{ΔM/+} male mice, as shown in the immunohistochemistry (IHC) assay. The macrophages accumulated near ballooned hepatocytes and formed a crown-like structure¹² (Figure 3G). Sirius Red staining indicated that the NASH livers of *Ncoa5*^{ΔM/+} male mice also had fibrosis (Figure 3H). We then examined the expression of the transcription factors PPARγ, SREBP-1c, and ChREBP, which are important in regulating hepatic glucose and lipid metabolisms and are often dysregulated in patients with NAFLD/NASH.^{13–15} Among them, the mRNA level of *Pparg2* was significantly increased in the livers of 10-month-old *Ncoa5*^{ΔM/+} mice compared with age-matched *Ncoa5*^{fl/+} male mice (Figure 4A). The protein level of PPARγ was elevated considerably and translocated to the nuclei in hepatocytes of *Ncoa5*^{ΔM/+} mice (Figure 4B). Consistent with this observation, the mRNA levels of the downstream targets of PPARγ2, including *G6pc*, *Fasn*, *Acaca*, *Plin2*, *Cd36*, and *Cidec*,¹⁶ were significantly increased in the livers of *Ncoa5*^{ΔM/+} male mice compared with *Ncoa5*^{fl/+} male mice (Figure 4C). Consistent with the previous report in *Ncoa5*^{+/-} male mice,¹⁰ *p21*^{cip1/waf1} expression was also increased in *Ncoa5*^{ΔM/+} male mice (Figure 4D). These results suggest that *Ncoa5*^{ΔM/+} male mice developed NASH at 10 months old.

Ncoa5-Deficient Macrophages Trigger Lipid Accumulation in Hepatocytes by Inducing the Expression of Lipogenic Genes, at Least in Part, Via Releasing PF4

To identify potential NCOA5 downstream targets and molecular factors in myeloid-lineage cells contributing to the development of NASH, we systematically examined genes and pathways altered in *Ncoa5*-deficient mice by performing RNA sequencing (RNA-seq) and transcriptome analysis on intrahepatic F4/80+ macrophages isolated from the pre-NASH livers of 6.5-month-old *Ncoa5*^{ΔM/+} and *Ncoa5*^{fl/+} male mice (Figure 5A and B). We found 207 differently expressed genes (DEGs) (fold change > 2, *P* adjusted < .1) between these 2 macrophage groups (Figure 5C) and that the genes encoding secretory proteins, including *Pf4*, *Angptl7*, and *Mmp13*, were up-regulated in *Ncoa5*^{ΔM/+} intrahepatic macrophages. *Pf4*, also known as chemokine CXCL4, was the most significantly increased among them. Interestingly, RNA-seq did not detect a significant change in the gene encoding the proinflammatory cytokine interleukin (IL) 6, which plays a critical role in the

initiation and progression of HCC in several mouse models of NASH and HCC, including *Ncoa5*^{+/-} male mice and diet- or chemical-induced mice.^{17,18} Moreover, the mRNA level of *Tnf* encoding another proinflammatory cytokine, tumor necrosis factor (TNF) α, was significantly reduced in the intrahepatic macrophages of *Ncoa5*^{ΔM/+} male mice, validated by real-time quantitative polymerase chain reaction (RT-qPCR) (Figure 5D). The expression of *Il6* or *Tnf* was comparable in the livers of *Ncoa5*^{ΔM/+} male mice compared with *Ncoa5*^{fl/+} mice at an earlier age (Figure 5E), indicating that these 2 proinflammatory cytokines may not be involved in the initiation of hepatic steatosis in these mice.

Because of the previous findings that CXCR3, a chemokine receptor for CXCL9, CXCL10, CXCL11, and PF4, was crucial in developing diet-induced NAFLD/NASH¹⁹ and among these ligands, only PF4 was overexpressed in *Ncoa5*^{ΔM/+} macrophages in RNA-seq data analysis (Figure 6A), we next focused on PF4. We confirmed that *Pf4* mRNA expression was increased in the intrahepatic macrophages of *Ncoa5*^{ΔM/+} male mice compared with age-matched *Ncoa5*^{fl/+} male mice by RT-qPCR (Figure 6B) and showed that the protein level of PF4 was also elevated in the NASH livers of *Ncoa5*^{ΔM/+} male mice compared with age-matched *Ncoa5*^{fl/+} male mice by Western blotting (Figure 6C). In contrast, PF4 expression was seemingly not elevated because it is undetectable in the livers of age-matched *Ncoa5*^{ΔM/+} and *Ncoa5*^{fl/+} female mice (Figure 6D). Interestingly, the expression of *Cxcr3* was also increased in the intrahepatic macrophages of *Ncoa5*^{ΔM/+} male mice (Figure 6E). *Pf4* was previously revealed as a continuously up-regulated gene in intrahepatic macrophages of NAFLD mice induced by a Westernized and sucrose/fructose-supplemented diet.²⁰ To determine whether *Pf4* is also up-regulated in other mouse models of NAFLD/NASH, we reanalyzed a published single-cell RNA-seq data set of nonparenchymal cells from Amylin liver NASH (AMLN) diet-induced NASH livers and normal diet-fed mouse livers.²¹ The t-SNE plots showed a liver cell clustering pattern and increased macrophage proportion in NASH livers similar to the previous reports (Figure 7A and B). Indeed, *Pf4* expression was significantly up-regulated in the intrahepatic macrophages from NASH livers compared with those from normal livers (Figure 7C). The high *Pf4* expression was found in Kupffer cells rather than in monocyte-derived macrophages (Figure 7C).

To determine the role of PF4 secreted from intrahepatic macrophages in hepatic lipogenesis regulation, we assessed the effect of macrophage PF4 on hepatocytes in vitro and in vivo. First, we demonstrated that *Ncoa5*-null macrophage-like RAW 264.7 cells displayed an increased PF4 expression

Figure 2. (See previous page). Development of metabolic-related phenotypes and spontaneous HCCs in *Ncoa5*^{ΔM/+} mice fed a normal diet. (A and B) GTT of 7-week-old (left) and ITT of 8-week-old (right) *Ncoa5*^{fl/+} and *Ncoa5*^{ΔM/+} male (A) and female (B) mice. Number of mice tested is labeled. (C) Body weight of 5-month-old *Ncoa5*^{fl/+} (*n* = 7) and *Ncoa5*^{ΔM/+} (*n* = 5) male mice. (D) Representative H&E staining photos of 5-month-old *Ncoa5*^{fl/+} and *Ncoa5*^{ΔM/+} males showing mild microvesicular steatosis in some 5-month-old *Ncoa5*^{ΔM/+} male mice. Scale bars: 50 μm and 750 μm (insert). (E) Incidence of HCC in aged *Ncoa5*^{fl/+} (*n* = 12) and *Ncoa5*^{ΔM/+} (*n* = 16) male mice monitored until 18 months old. (F) Representative macroscopic photos and H&E-stained liver sections of 18-month-old *Ncoa5*^{fl/+} or tumor-bearing *Ncoa5*^{ΔM/+} male mice. Red circles indicate HCCs. Scale bar: 1 cm, 100 μm, or 50 μm. Data represent mean ± SEM. Two-tailed unpaired *t* test. **P* < .05.

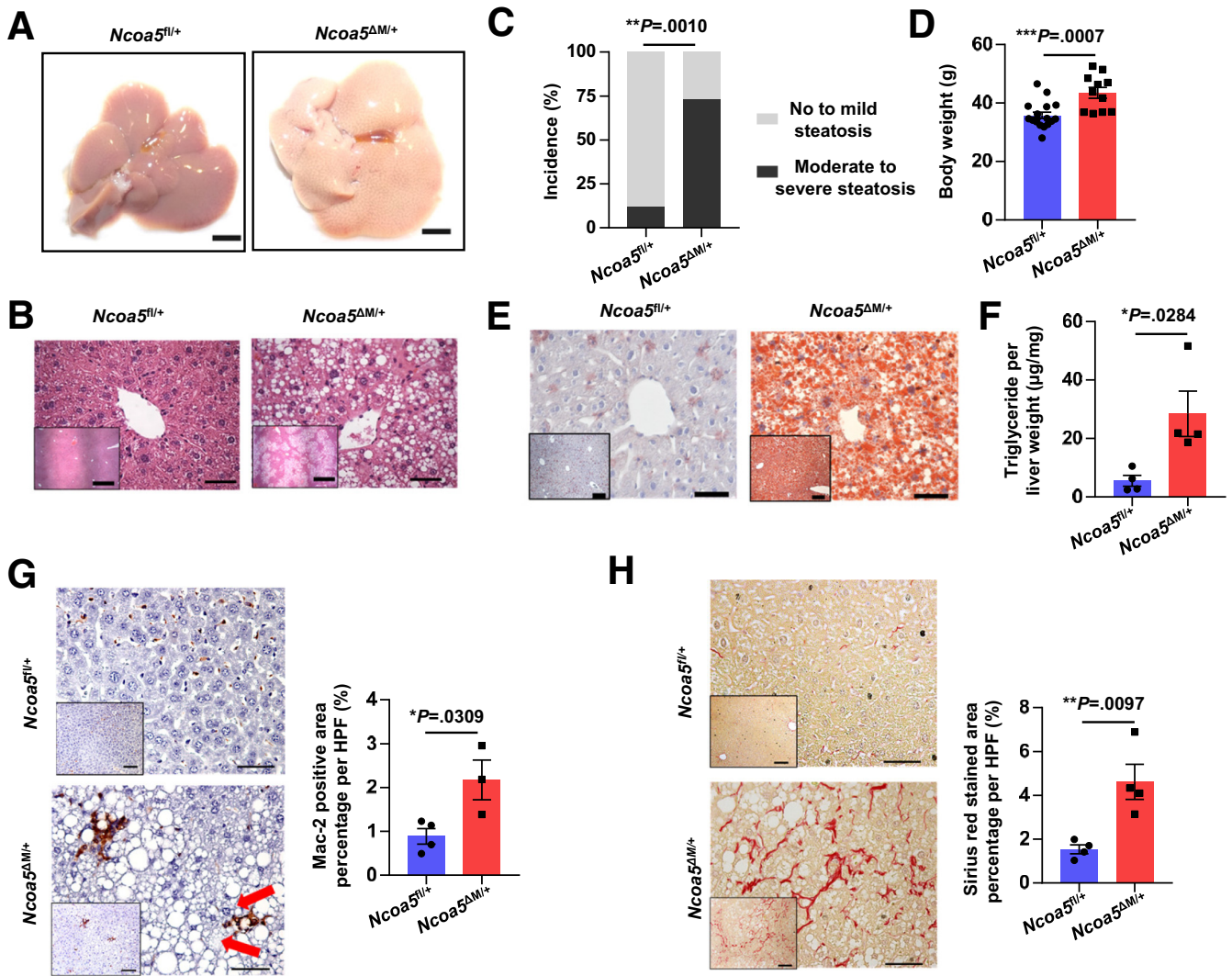


Figure 3. Phenotypes in livers of 10-month-old *Ncoa5^{ΔM/+}* male mice fed a normal diet. (A) Representative macroscopic images of liver from 10-month-old *Ncoa5^{fl/+}* and *Ncoa5^{ΔM/+}* male mice. Scale bar: 0.5 cm. (B) Representative H&E staining of liver sections from 10-month-old *Ncoa5^{fl/+}* and *Ncoa5^{ΔM/+}* male mice. Scale bar: 50 μ m or 750 μ m (insert). (C) Incidence of no to mild steatosis and moderate to severe steatosis in 10-month-old *Ncoa5^{fl/+}* (n = 17) and *Ncoa5^{ΔM/+}* (n = 11) male mice. χ^2 test. (D) Body weight of 10-month-old *Ncoa5^{fl/+}* (n = 17) and *Ncoa5^{ΔM/+}* (n = 11) male mice. (E) Representative Oil-Red-O staining of livers from 10-month-old *Ncoa5^{fl/+}* and *Ncoa5^{ΔM/+}* male mice. Scale bar: 50 μ m or 200 μ m (insert). (F) Liver triglyceride concentration of mice as indicated. Mice, n = 4 for each group. (G) Representative images of Mac-2 IHC liver sections from 10-month-old *Ncoa5^{fl/+}* (n = 4) and *Ncoa5^{ΔM/+}* (n = 3) male mice and quantification of stained area positive for Mac-2. Arrow indicates hepatocytes with ballooning. 5 HPFs per mouse. Scale bar: 50 μ m and 100 μ m. (H) Representative images of Sirius Red-stained sections from 10-month-old *Ncoa5^{fl/+}* (n = 4) and *Ncoa5^{ΔM/+}* (n = 4) male mice and quantification of stained areas. 5 HPFs per mouse. Scale bar: 50 μ m and 100 μ m. Data represent mean \pm SEM. Two-tailed unpaired t test was used if not otherwise specified. * $P < .05$, ** $P < .01$, *** $P < .001$.

compared with control RAW264.7 cells (Figure 8A). Media conditioned by different RAW264.7 cells that contain various secreted factors were collected for treating hepatocytes. We showed that cellular lipids were significantly increased in primary mouse hepatocytes and human HepG2 cells treated with the conditioned medium (CM) of *Ncoa5*-null RAW 264.7 cells compared with those treated with the CM of vector-control RAW 264.7 cells (Figure 8B and C). Next, we demonstrated that treating HepG2 cells with the CM of *Ncoa5*-null RAW 264.7 cells significantly increased expression of *FASN*, which encodes the key enzyme fatty

acid synthase in lipogenesis, compared with those treated with the CM of vector-control RAW 264.7 cells (Figure 9A). Importantly, treating HepG2 cells with recombinant mouse PF4 had a similar effect (Figure 9B). To determine whether the effect of CM treatment on *FASN* expression was due to PF4 overexpression, we generated *Ncoa5*-null RAW 264.7 cells with or without *Pf4* knockdown (Figure 9C). Mouse primary hepatocytes treated with the CM from the *Ncoa5*-null RAW 264.7 cells with *Pf4* knockdown had significantly lower *Fasn* expression than those treated with the CM from the *Ncoa5*-null cells transfected with a control small

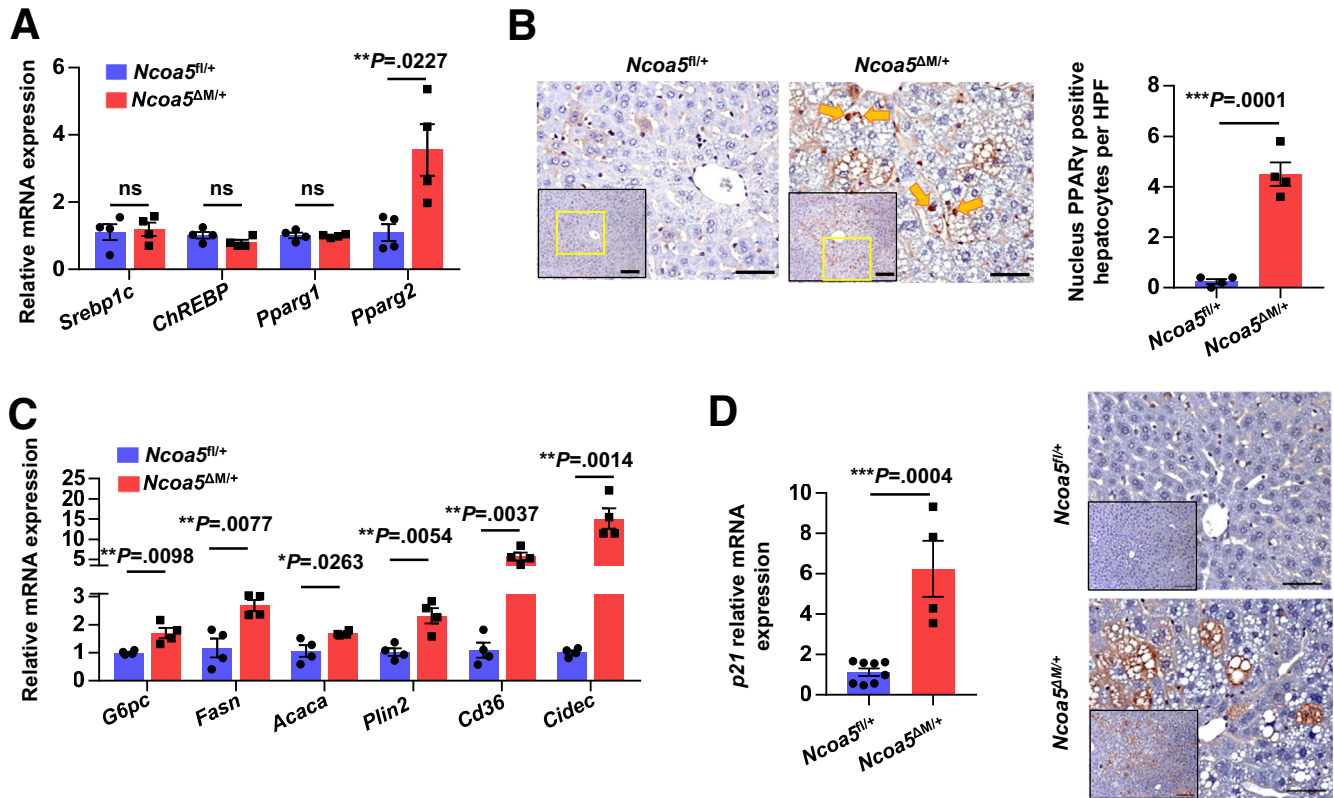


Figure 4. Steatosis-related gene expression in *Ncoa5^{ΔM/+}* male mice fed a normal diet. (A) RT-qPCR analysis of mRNA expression levels of transcription factors related to liver lipid metabolism between livers of 10-month-old *Ncoa5^{fl/+}* ($n = 4$) and *Ncoa5^{ΔM/+}* ($n = 4$) male mice. (B) Representative images of IHC for PPAR γ in liver sections of 10-month-old *Ncoa5^{fl/+}* ($n = 4$) and *Ncoa5^{ΔM/+}* ($n = 4$) male mice and quantification of nucleus-positive cell numbers. Arrows indicate nuclear localization of PPAR γ . (C) RT-qPCR analysis of mRNA levels of genes encoding critical enzymes in glucose and lipid metabolisms and genes regulated by PPAR γ in the liver of 10-month-old *Ncoa5^{fl/+}* ($n = 4$) and *Ncoa5^{ΔM/+}* ($n = 4$) male mice. (D) RT-qPCR analysis of mRNA expression levels of *p21* in livers of 10-month-old *Ncoa5^{fl/+}* ($n = 8$) and *Ncoa5^{ΔM/+}* ($n = 4$) male mice and representative photos of IHC for *p21*. Data represent mean \pm SEM. Two-tailed unpaired *t* test. **P* < .05, ***P* < .01, ****P* < .001. Scale bar: 50 μ m and 100 μ m (insert).

interfering RNA (siRNA) (Figure 9D). Moreover, we ectopically overexpressed human or mouse *PF4* in RAW 264.7 cells and used their CM to treat mouse primary hepatocytes (Figure 9E). The CM from either mouse or human *PF4*-overexpressed cells was able to increase lipid content and the mRNA levels of *G6pc* and *Acaca*, encoding key enzymes in glucose neogenesis and lipogenesis, in primary mouse hepatocytes (Figure 9F and 9G) and increased the triglyceride concentration in HepG2 cells (Figure 9H) compared with CM from RAW 264.7 cells that express green fluorescent protein control. Mouse primary hepatocytes treated with recombinant mouse *PF4* significantly increased the mRNA expressions of *G6pc*, *Cyp2e1*, *Fasn*, *p21*, and *Acaca* and trended to increase the triglyceride content (Figure 9I and J). Finally, we used a glucan-encapsulated siRNA particle (GeRP) approach^{22–24} to specifically target intrahepatic macrophages in mice (Figure 10A and B), using a siRNA that efficiently knocks down *Pf4* expression in vitro (si3 in Figure 10C). *PF4* overexpression was confirmed in the intrahepatic macrophages of mice fed the aforementioned Westernized diet²⁰ (Figure 10D). Specific *Pf4* knockdown in intrahepatic macrophages (Figure 10E) reduced the lipid

accumulation, and the mRNA levels of *Pparg2* and its downstream targets in the livers of mice fed the Westernized diet (Figure 10F–I). The reduction in the mRNA levels of *Pparg2* and its downstream targets by the *Pf4* knockdown was also observed in the livers of male *Ncoa5^{ΔM/+}* mice (Figure 10J). Altogether, these results suggest that increased *PF4* from intrahepatic macrophages triggers the onset of hepatic steatosis via increasing expression of lipogenic genes in male *Ncoa5^{ΔM/+}* mice and a diet-induced model of NAFLD with reported *Pf4* up-regulation specifically in intrahepatic macrophages.

Dysregulated Intrahepatic Macrophages From *Ncoa5^{ΔM/+}* Male Mice Highly Resemble the Intrahepatic Macrophages From NAFLD Humans

To determine the clinical relevance of our findings, we compared the dysregulated transcriptomes between intrahepatic macrophages from *Ncoa5^{ΔM/+}* mice and humans with obesity or NAFLD. Generally Applicable Gene-set Enrichment (GAGE) analysis²⁵ revealed 47 up-regulated and 41 down-regulated Kyoto encyclopedia of genes and

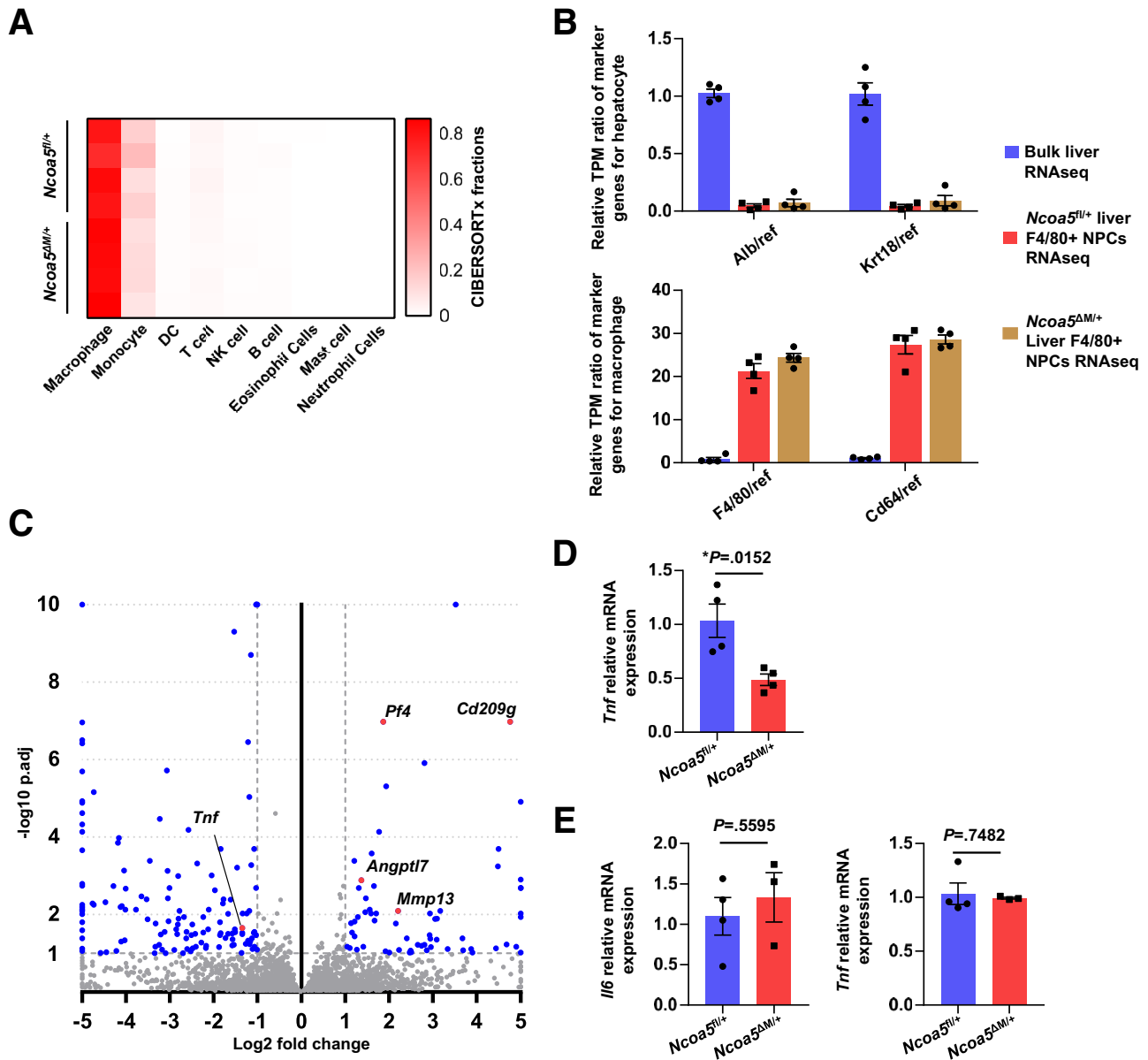


Figure 5. Expression difference of classic proinflammatory cytokines comparing *Ncoa5^{fl/+}* and *Ncoa5^{ΔM/+}* intrahepatic macrophages. (A) Cell-type composition of isolated F4/80+ hepatic nonparenchymal cells from 6.5-month-old *Ncoa5^{fl/+}* and *Ncoa5^{ΔM/+}* males inferred by CIBERSORTx using immuCC signature. (B) Relative expression of hepatocyte and macrophage markers in isolated F4/80+ hepatic nonparenchymal cells from 6.5-month-old *Ncoa5^{fl/+}* and *Ncoa5^{ΔM/+}* males compared with bulk livers from 5-month-old wild-type C57BL/6 males (GSE110524). $n = 4$ per mouse group. Relative expression of marker genes was calculated as the transcripts per million (TPMs) of markers divided by TPMs of a group of housekeeping genes and then normalized to the result of bulk liver RNA-seq. Data represent mean \pm SEM. (C) Volcano plot showing DESeq2 differential gene expression analysis results compared the intrahepatic macrophages from 6.5-month-old *Ncoa5^{fl/+}* males versus *Ncoa5^{ΔM/+}* males. Genes with P adjusted < .1 and fold-change > 2 were labeled in blue. (D) RT-qPCR validation of *Tnf* mRNA expression in intrahepatic macrophages from 6.5-month-old *Ncoa5^{fl/+}* ($n = 4$) and *Ncoa5^{ΔM/+}* ($n = 4$) male mice. (E) RT-qPCR analysis of mRNA levels of *Il6* and *Tnf* in livers of 3-month-old *Ncoa5^{fl/+}* ($n = 4$) and *Ncoa5^{ΔM/+}* ($n = 3$) male mice. Data represent mean \pm SEM. Two-tailed unpaired t test. * $P < .05$.

genomes (KEGG) pathways ($q < 0.1$), including up-regulated fatty acid metabolism and fatty acid elongation pathways, in *Ncoa5^{ΔM/+}* intrahepatic macrophages (Figure 11A). When applying the same pathway analysis to the transcriptome data of human intrahepatic macrophages

from non-obese and obese individuals,²⁴ we found that 60.2% of dysregulated KEGG pathways in *Ncoa5^{ΔM/+}* intrahepatic macrophages were also dysregulated in the intrahepatic macrophages of obese humans in the same direction ($q < 0.1$) (Figure 11A). Unlike mouse cells, the

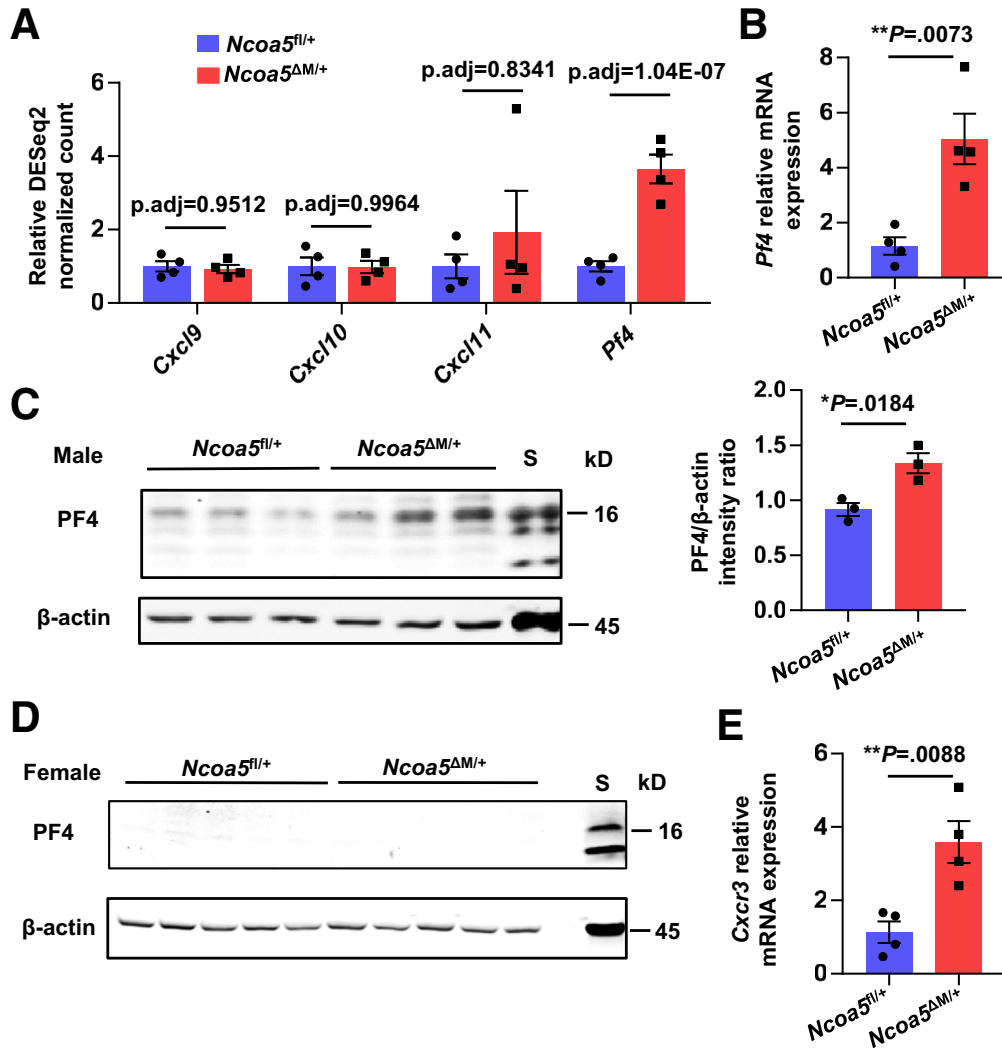


Figure 6. Expression changes of CXCR3 and its ligands in *Ncoa5^{ΔM/+}* male mice fed a normal diet. (A) The mRNA levels of genes encoding CXCR3 ligands in intrahepatic macrophages from 6.5-month-old *Ncoa5^{fl/+}* and *Ncoa5^{ΔM/+}* males. They were assessed by RNA-seq and shown as DESeq2 normalized counts relative to average counts of *Ncoa5^{fl/+}* male mice (as 1). *P* adjusted calculated by DESeq2. (B) RT-qPCR validation of *Pf4* mRNA expression in intrahepatic macrophages from 6.5-month-old *Ncoa5^{fl/+}* ($n = 4$) and *Ncoa5^{ΔM/+}* ($n = 4$) male mice. (C) Western blotting and quantification of PF4 protein level in liver lysates of 10-month-old *Ncoa5^{fl/+}* ($n = 3$) and *Ncoa5^{ΔM/+}* ($n = 3$) male mice. S, spleen lysate from wild-type mice. (D) Western blotting of PF4 protein level in liver lysates of 5-month-old *Ncoa5^{fl/+}* ($n = 5$) and *Ncoa5^{ΔM/+}* ($n = 5$) female mice. S, spleen lysate from wild-type mice. (E) RT-qPCR validation of *Cxcr3* mRNA expression in intrahepatic macrophages from 6.5-month-old *Ncoa5^{fl/+}* ($n = 4$) and *Ncoa5^{ΔM/+}* ($n = 4$) male mice. Data represent mean \pm SEM. Two-tailed unpaired *t* test if not otherwise specified. **P* < .05, ***P* < .01.

human cell also expresses a PF4 variant 1 gene (*PF4V1*) that encodes a protein in the mature form 96% identical to mature PF4. We found that most obese individuals had highly up-regulated PF4 or PF4V1 mRNA expression in their intrahepatic macrophages compared with non-obese individuals (Figure 11B). Next, we generated the NCOA5-MΔ signature using the high-confidential human homologs (156 genes, Table 1) converted from *Ncoa5^{ΔM/+}* hepatic macrophage DEGs (171 genes with Entrez Gene ID within the 207 DEGs) and applied this signature to human NAFLD patient and healthy control liver transcriptome data using single-sample gene set enrichment analysis (ssGSEA).^{26,27} The enrichment score of this signature was significantly higher in NAFLD patient livers (Figure 11C). It significantly correlated with

most NAFLD clinical parameters, including alanine transaminase (ALT), steatosis area, liver docosahexaenoic acid of total lipid, and others (Figure 11D). These data indicated that dysregulated intrahepatic macrophages from *Ncoa5^{ΔM/+}* male mice resembled those from obese people or NAFLD patients. We also found that NAFLD patients, including those with NASH, did not have apparent hepatic inflammation in this human liver gene expression data set (Figure 12).

Ncoa5 Deficiency Promotes the Differentiation of Macrophages Toward M2-Like

We previously reported increased M2 macrophage infiltration in the preneoplastic liver of *Ncoa5^{+/-}* male

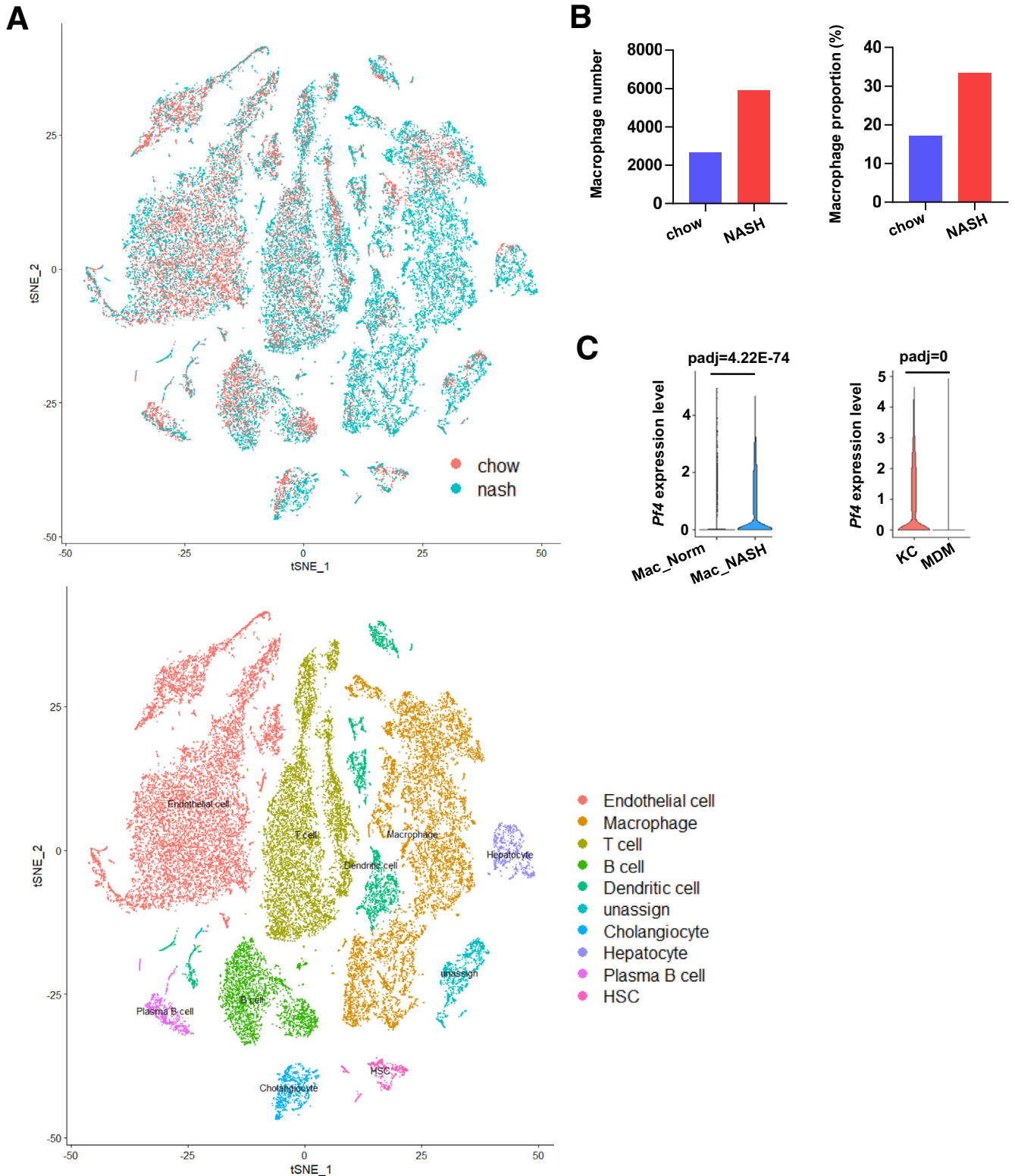


Figure 7. Difference of *Pf4* expression of AMLN diet and control diet mice assessed by single-cell RNA-seq. (A) t-SNE plot visualizing the single-cell transcriptome clustering of liver cells from mice fed a control diet (chow) and mice fed an AMLN diet (NASH); *top*, cells labeled according to mouse diets; *bottom*, cells labeled according to inferred cell types. (B) Cell number and proportion of inferred macrophage cell type in mice fed a control diet (chow) and an AMLN diet (NASH). They were produced in our re-analysis of the NCBI Sequence Read Archive PRJNA531644 raw data. (C) *Pf4* expression in intrahepatic macrophages of AMLN-induced NASH livers and control livers (GSE129516). Seurat reported adjusted *P* values. KC, Kupffer cell; Mac, intrahepatic macrophage; MDM, monocyte-derived macrophage.

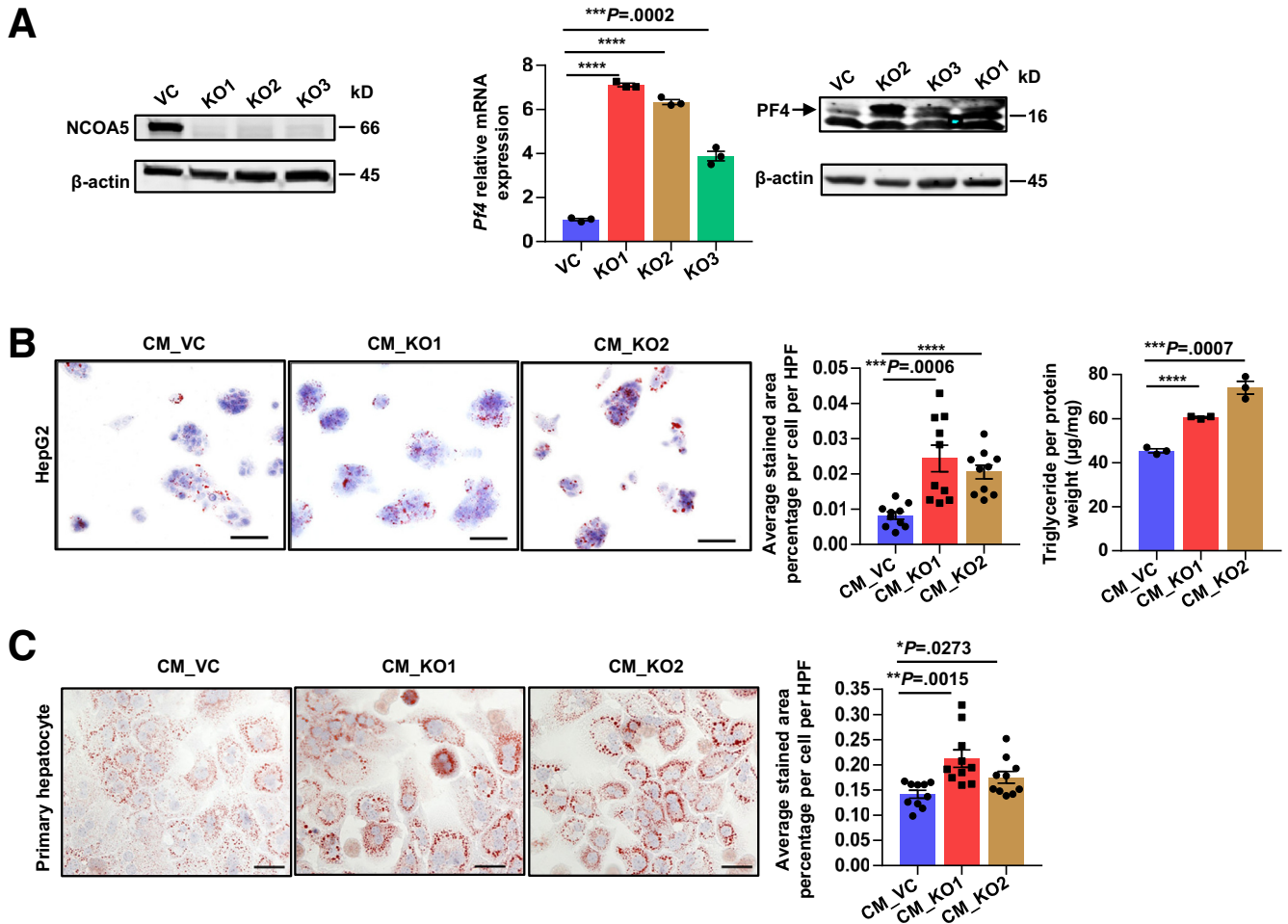


Figure 8. Effect of *Ncoa5* knockout on PF4 expression in macrophage-like RAW 264.7 cells and the influence of their CM to lipid accumulation in hepatocytes. (A) *Left*: Western blot validation of *Ncoa5* knockout in RAW 264.7 cells. KO1-3, 3 independent clones; VC, vector control. *Mid and right*: RT-qPCR showing *Pf4* mRNA levels (*mid*) and Western blotting analyzing PF4 protein (*right*) in RAW 264.7 cells with or without *Ncoa5* knockout. PF4 is indicated with arrow. (B) *Left*: Representative Oil-Red-O staining of human HCC HepG2 cells treated with CM from RAW 264.7 cells with or without *Ncoa5* knockout for 1 day. *Middle*: Quantification of Oil-Red-O-stained area per cell treated with indicated CM, 5 HPFs were captured in each condition, combined results from 2 experiments. *Right*: Cell triglyceride concentration of HepG2 cells treated with indicated CM. Representative data of 3 repeats. Data were quantitated and expressed as micrograms of triglyceride per milligram of protein. (C) Representative Oil-Red-O staining and quantification of stained area per cell for mouse primary hepatocytes treated with CM from RAW 264.7 cells with or without *Ncoa5* knockout for 1 day. 5 HPFs were captured in each condition, combining results from 2 experiments. Scale bar: 50 μ m. Data represent mean \pm SEM. Two-tailed unpaired *t* test. $*P < .05$, $**P < .01$, $***P < .001$, $****P < .0001$.

mice.^{9,10} Consistently, our pathway analysis revealed that proinflammatory pathways, including TNF signaling, nuclear factor kappa B signaling, and toll-like receptor signaling, were down-regulated in *Ncoa5*^{ΔM/+} intrahepatic macrophages. In contrast, anti-inflammatory PPAR signaling²⁸ was up-regulated (Figure 11A). These results agree with the aforementioned observation that the expression of TNF α , an M1 macrophage marker, was significantly reduced in the intrahepatic macrophages of *Ncoa5*^{ΔM/+} male mice (Figure 5D), indicating a transition to M2-like differentiation. M2-like macrophages have a repertoire of tumor-promoting capabilities such as inducing an immunosuppressive microenvironment and promoting the growth and

metastatic potential of cancer cells. We sought to determine whether myeloid-lineage-specific heterozygous deletion of *Ncoa5* in mice is sufficient to increase the intrahepatic M2-like macrophage population observed previously in *Ncoa5*^{+/-} male mice,¹⁰ which might contribute to the formation of the hepatic immunosuppressive microenvironment in *Ncoa5*^{ΔM/+} male mice. Transcriptome analysis indicated that the intrahepatic macrophages of pre-NASH *Ncoa5*^{ΔM/+} male mice expressed significantly higher levels of Cd209 family genes, markers for M2 macrophages (Figure 13A). The increased M2-like macrophages in the livers of *Ncoa5*^{ΔM/+} male mice were confirmed by IHC using an antibody against mouse M2 macrophage marker YM1

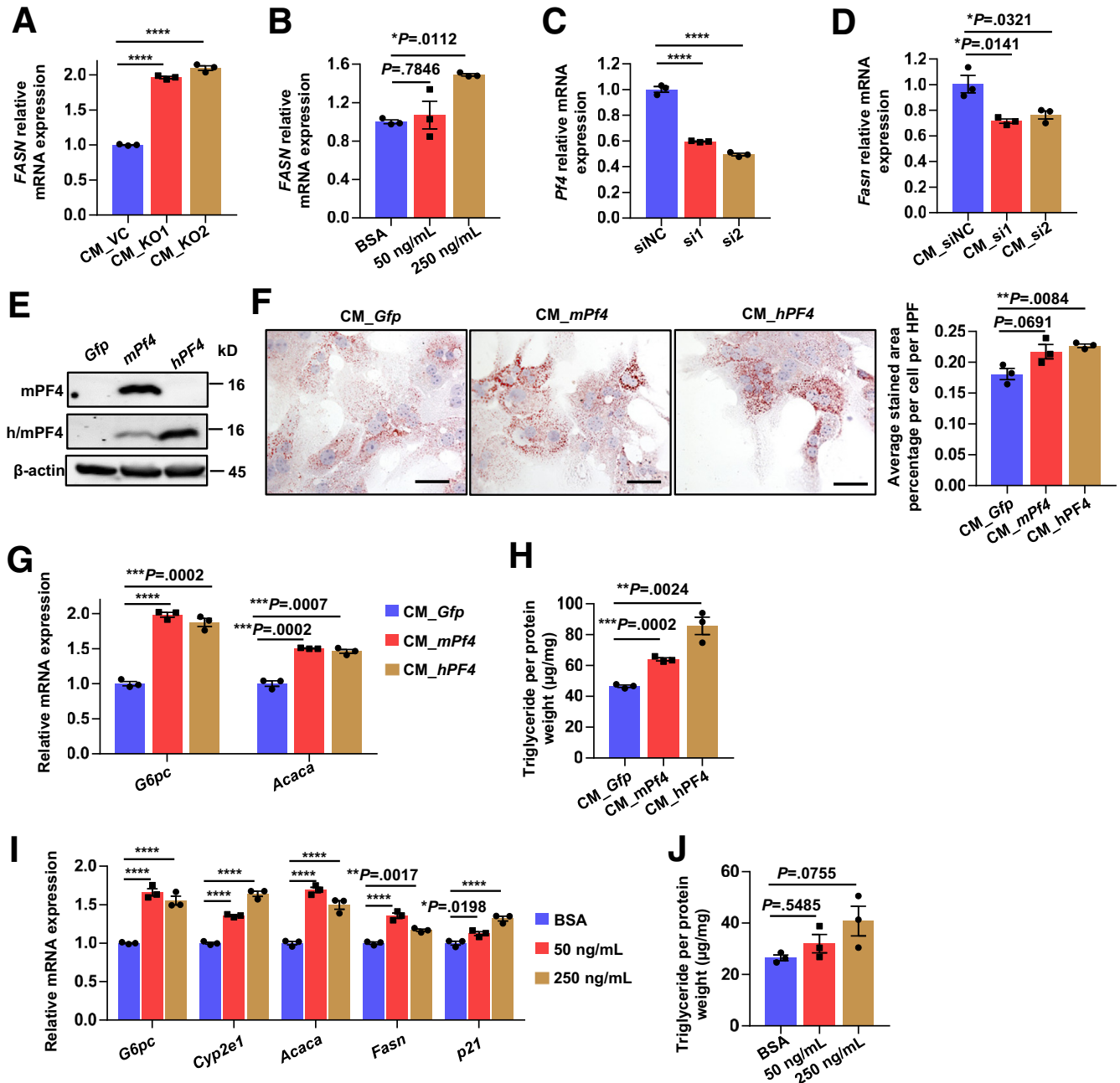
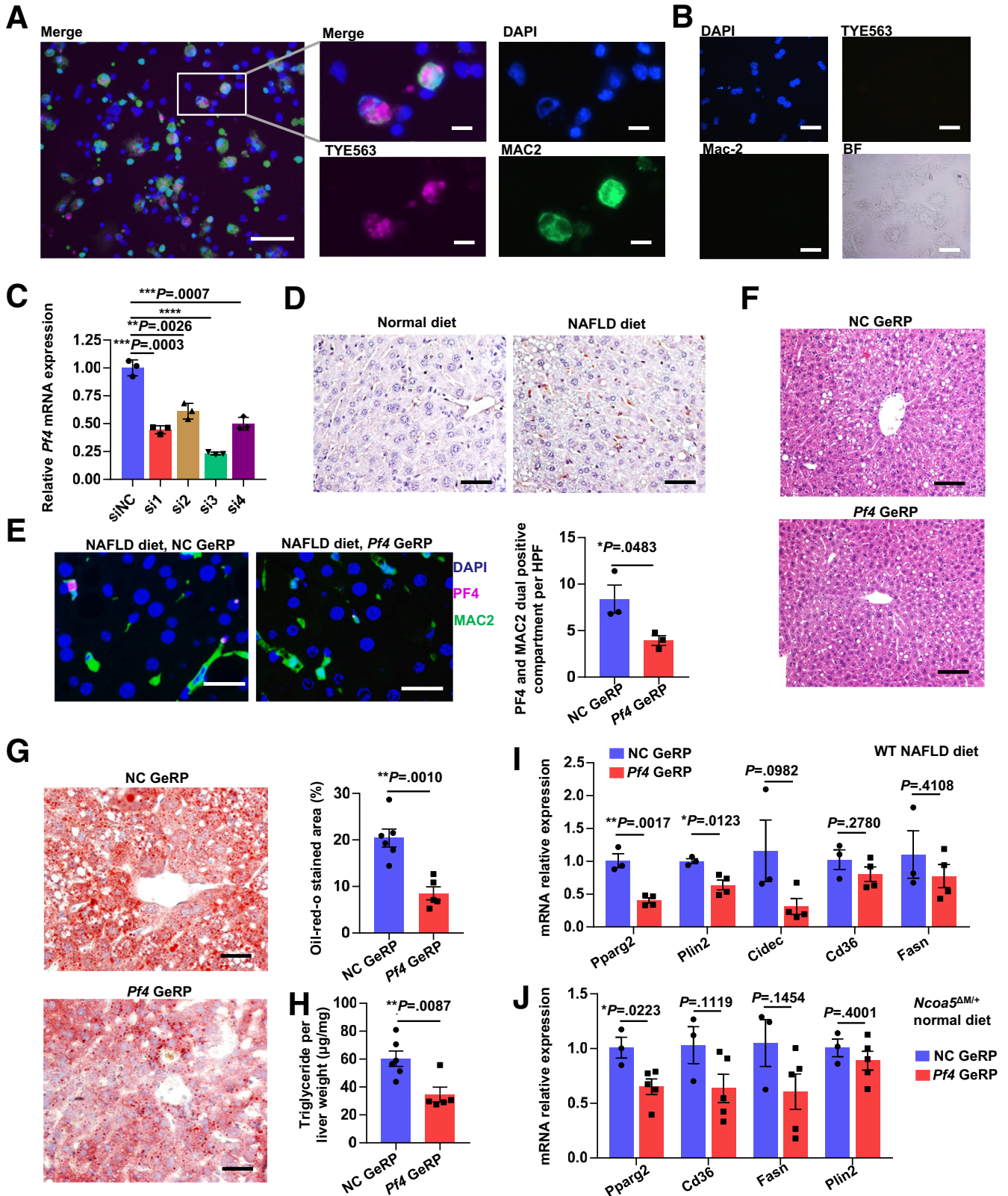


Figure 9. Effects of PF4 on lipid accumulation and lipogenic gene expression in the hepatocyte. (A) RT-qPCR analysis of mRNA levels of *Fasn* in HepG2 cells treated with CM from RAW 264.7 cells with or without *Ncoa5* knockout. (B) RT-qPCR analysis of mRNA levels of *FASN* in HepG2 cells treated with bovine serum albumin (BSA) or recombinant mouse PF4 in low glucose 5% fetal bovine serum medium for 3 days. One-way analysis of variance Dunnett's multiple comparisons test. (C) RT-qPCR analysis of *Pf4* mRNA levels in *Ncoa5*-null RAW 264.7 cells transfected with siRNAs for *Pf4* or negative control siRNA (siNC). (D) RT-qPCR analysis of mRNA expression of *Fasn* in mouse primary hepatocytes treated with CM from *Ncoa5*-null RAW 264.7 cells with or without *Pf4* knockdown. (E) Western blotting validation of mouse PF4 overexpression or human PF4 ectopic expression in lentivirus-transformed RAW 264.7 cells. h/mPF4, an antibody that recognizes both human and mouse PF4. (F) *Left*: Representative Oil-Red-O staining images of mouse primary hepatocytes treated with CM from RAW 264.7 cells with or without PF4 overexpression. *Right*: Quantification of stained area per cell. 5 HPFs were captured in each condition, summarized from 3 repeats. (G) RT-qPCR analysis of *G6pc* and *Acaca* mRNA expression in mouse primary hepatocytes treated with CMs from RAW 264.7 cells with PF4 ectopic expression. Representative data from 3 repeats. (H) Cell triglyceride concentration per protein weight of HepG2 cells treated with different CMs. Representative data from 3 repeats. Data were quantitated and expressed as micrograms of triglyceride per milligram of protein. (I) RT-qPCR analysis of mRNA levels of glucose and lipid metabolism genes in mouse primary hepatocytes treated with recombinant mouse PF4. Two-way analysis of variance Dunnett's multiple comparisons test. (J) Cell triglyceride concentrations in mouse primary hepatocytes treated with recombinant mouse PF4. Data were quantitated and expressed as micrograms of triglyceride per milligram of protein. Data represent mean \pm SEM. Two-tailed unpaired *t* test was used if not otherwise specified. * $P < .05$, ** $P < .01$, *** $P < .001$, **** $P < .0001$. Scale bar: 50 μ m.

(Figure 13B). To verify that the transition to M2-like macrophages was caused by *Ncoa5* deficiency intrinsically, we isolated peritoneal macrophages from 6-week-old *Ncoa5*^{f1/+}

and *Ncoa5*^{ΔM/+} male mice and assessed the expression of M2 macrophage markers. Without external stimulation, elevated expression of *Arg1*, *Il10*, and *Ym1* was already



evident in peritoneal macrophages from *Ncoa5*^{ΔM/+} male mice compared with *Ncoa5*^{fl/+} male mice (Figure 13C). When treated with IL-4 and IL-13 to induce M2 differentiation, the peritoneal macrophages from *Ncoa5*^{ΔM/+} male mice expressed higher *Arg1* and *Ym1* mRNA than those from *Ncoa5*^{fl/+} male mice (Figure 13D).

Because PF4 treatment could induce monocyte differentiation into macrophages and reduce the M1 activation of mouse macrophages,^{29–31} we asked whether *Pf4* overexpression affects M2-like differentiation of macrophages. RAW 264.7 cells with *Pf4* overexpression or ectopic human PF4 expression had significantly increased expression of *Arg1* and *Il10*, two M2 markers, whereas treating cells with M2-inducers resulted in higher *Arg1* and *Il10* expression in cells with PF4 overexpression (Figure 13E). Treating RAW 264.7 cells with recombinant mouse PF4 significantly increased *Arg1* expression (Figure 13F). These results suggest a role of PF4 in inducing macrophage M2-like differentiation.

Macrophages Lacking NCOA5 Affect HCC Cell Growth and Invasion Potential in Vitro

M2-like macrophages can promote tumor cell proliferation and metastasis potential.^{32,33} We then examined the effect of *Ncoa5*-deficient macrophages on HCC cell growth and invasion potential in vitro by treating HepG2 cells with CM of RAW 264.7 cells with or without *Ncoa5* knockout. HepG2 cells treated with CM of *Ncoa5*-null RAW 264.7 cells had increased cell growth compared with cells treated with CM of control RAW 264.7 cells (Figure 14A). CM of *Ncoa5*-null RAW 264.7 cells could promote HepG2 cell migration compared with CM of control RAW 264.7 cells (Figure 14B). CM of *Ncoa5*-null RAW 264.7 cells increased the AKT phosphorylation in HepG2 cells compared with CM of control RAW 264.7 cells, suggesting that the increased growth and migration might be related to AKT activation (Figure 14C). Together, these results indicate that macrophages with NCOA5 loss promote HCC cell growth and invasion in vitro.

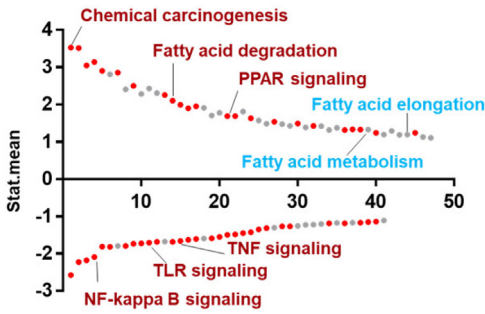
High PF4 Expression in Human HCC Samples Correlated With Poor Overall Survival and Increased M2 Macrophages, Regulatory T Cells, and Myeloid-Derived Suppressor Cells in HCCs

PF4 was demonstrated to stimulate the proliferation of regulatory T cells (Tregs) and induce the tumor-infiltrated populations of myeloid-derived suppressor cells (MDSCs), which could suppress the activation, proliferation, and cytokine production of CD4+ and CD8+ T cells and correlate negatively with cancer patient survival.^{34–36} To assess the clinical relevance of PF4 high expression in HCC, we analyzed The Cancer Genome Atlas (TCGA) liver hepatocellular carcinoma (LIHC) cohort and used the mRNA levels of PF4 and its non-allelic variant PF4V1 to segregate TCGA HCC patients. Kaplan-Meier analysis revealed that HCC patients with high tumoral combined PF4 and PF4V1 mRNA expression had a significantly worse overall survival than the rest of the HCC patients (Figure 15A). Next, CIBERSORTx was used to infer immune cell type proportions in HCCs from the same HCC patient cohort.³⁷ We found that the HCC samples with the high expression of combined PF4 and PF4V1 had significantly higher M2 macrophages fractions using the default LM22 signature (Figure 15B). Moreover, the positive correlation of combined PF4 and PF4V1 mRNA expression with M2 macrophage fractions was shown using CIBERSORTx (Figure 15C) and the xCell method (Figure 15D).³⁸ Although having a similar proportion of CD8 T-cell fraction (Figure 15B), HCCs with high PF4 and PF4V1 mRNA expression expressed higher immune checkpoint molecule *TIM3* and MDSC marker *CD84*³⁹ compared with the rest tumors (Figure 15E). The signatures of Treg⁴⁰ and MDSC³⁹ were enriched in HCCs with high PF4 and PF4V1 expression compared with the rest of the HCC samples⁴¹ (Figure 15F and G). In the LCI HCC cohort, an HCC cohort with a different patient ethnicity and etiology compared with the TCGA cohort,⁴² high tumoral PF4 and PF4V1 mRNA expression also correlated with poor overall survival and recurrence-free survival (Figure 16A), and tumors with high PF4 and PF4V1 expression also had increased *CD84* expression (Figure 16B). Furthermore, we found that HCC patients with high tumoral PF4 protein expression had poor

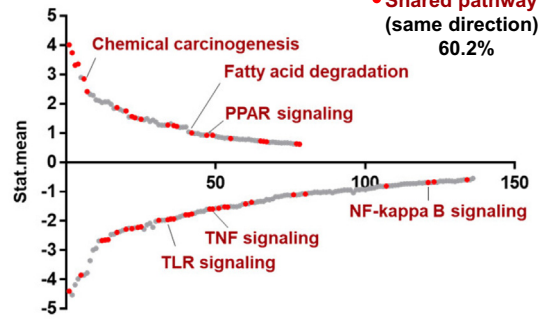
Figure 10. (See previous page). Effect of hepatic-macrophage-specific *Pf4* knockdown on hepatic steatosis in wild-type mice fed a NAFLD diet, and *Ncoa5*^{ΔM/+} fed a normal diet. (A and B) Representative immunofluorescence staining of Mac-2 in isolated hepatic non-parenchymal cells (A) or parenchymal cells (B) from mice injected with GeRPs containing TYE563-labeled siRNA. Blue: DAPI. Purple: TYE563. Green: Mac-2. Scale bar in (A) left: 50 μm, middle and right: 10 μm. Scale bar in (B): 50 μm. (C) RT-qPCR analysis of *Pf4* mRNA expression in RAW 264.7 *Ncoa5* knockout clone 1 treated with 4 different Dharmacon siRNAs targeting mouse *Pf4* (si1-si4) or a non-targeting siRNA (siNC). Two-tailed unpaired *t* test. (D) Representative IHC staining of PF4 in livers of wild-type male mice fed a normal or NAFLD diet for 3 months. Scale bar: 50 μm. (E) Representative dual-immunofluorescence staining of PF4 and Mac-2 in livers of wild-type male mice (n = 3 per group) fed a NAFLD diet injected with siNC- or si3-containing GeRPs and the quantification of dual-stained compartments. Blue: DAPI. Purple: PF4. Green: Mac-2. Two-tailed unpaired *t* test. (F) Representative H&E staining of livers from wild-type male mice fed a NAFLD diet injected with siNC- or si3-containing GeRPs. Scale bar: 100 μm. (G) Representative Oil-Red-O staining of livers from siNC- (n = 6) or si3-containing (n = 5) GeRPs injected wild-type male mice fed a NAFLD diet and quantification of Oil-Red-O-stained area. Scale bar: 50 μm. Two-tailed unpaired *t* test. (H) Triglyceride concentration of livers from siNC- (n = 6) or si3-containing (n = 5) GeRPs injected wild-type male mice fed a NAFLD diet. Two-tailed unpaired *t* test. (I) RT-qPCR analysis of mRNA expression of *Pparg2* and its target genes in livers of wild-type male mice fed a NAFLD diet injected with siNC- (n = 3) or si3-containing (n = 4) GeRPs. Two-tailed unpaired *t* test. (J) RT-qPCR analysis of mRNA expression of *Pparg2* and its target genes in livers of 7.5-month-old *Ncoa5*^{ΔM/+} male mice fed a normal diet injected with siNC- (n = 3) or si3-containing (n = 5) GeRPs. Two-tailed unpaired *t* test. *****P* < .0001, ****P* < .001, ***P* < .01, **P* < .05.

A

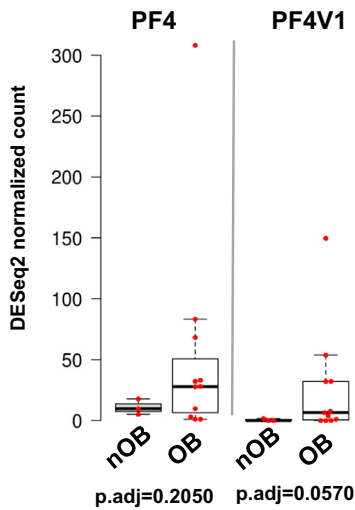
Mouse HMs, *Ncoa5^{ΔM/+}* vs *Ncoa5^{fl/+}*



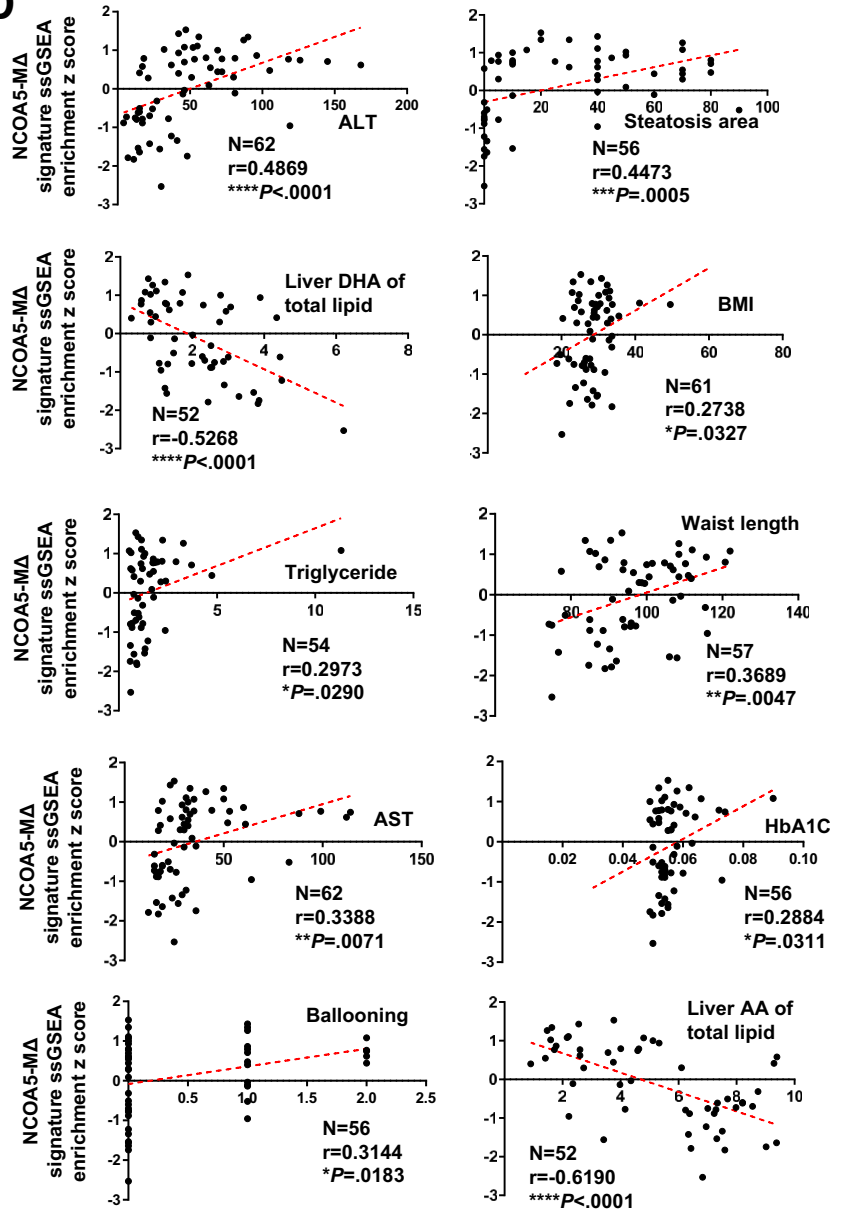
Human HMs, obese vs non-obese



B



D



C

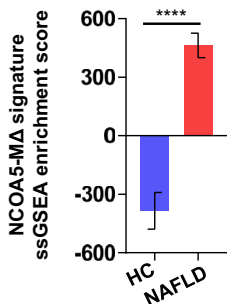


Table 1. NCOA5- Δ M Gene Signature

Up	ANGPTL7, BMP7, C20orf173, C8orf34, CACNG7, CCT6B, CD209, CD4, PF4, PF4V1, CIDEA, CLSTN3, DCT, FAM241B, FITM1, FRS3, GPRC5B, GSTM3, KLHL32, MMP13, MT-ATP6, NAT8, NAT8B, PIANP, POMGNT2, PTPRT, PXDC1, RAB34, RGS11, RIMKLB, SEMA5B, SGCE, SLC12A5, SLC1A2, SLC22A3, SMIM1, SPTLC3, SYNGAP1, TENM2, THRSP, TLX1, TPPP, UNC13B, ZNF627
Down	ABCB1, AC008012.1, AC010616.1, ACE, ADORA2B, AGPAT4, AL049634.2, AL357075.4, ANKDD1A, AP000781.2, ATP1A3, BCAS1, BCL2, BCL2A1, C3orf80, CCL18, CCL3, CCL3L3, CCND2, CD177, CD244, CD300E, CD79B, CLEC4E, CNN2, CORO1A, CYFIP2, DGKG, DNAH12, DUSP2, DUSP5, EGR3, EPHA4, FAM217B, FCGR3A, FCGR3B, FCRL5, FNDC1, FUT7, GDA, GFI1B, GLIPR1, GPR171, GPR18, GPR31, GRAP2, GRHL1, HCCS, IFIT1B, IGSF9, IKZF3, IL12B, IL21R, IPCEF1, ITGAD, ITGAX, KCNA3, KCNG3, KCNN4, KLRB1, KLRG2, KRT80, LAT2, LTBP2, MAP3K19, MBP, MCUB, MMP8, MSL3, MYO1E, NAPSA, NAT8L, NEGR1, NR4A2, NUPR1, NXPE3, NXPE4, PBXIP1, PCDHGA10, PDCD1, PECAM1, PLAUR, PPP1R3D, PRG2, PRPS2, PSTPIP1, RADX, RNF144A, RUNX2, RYR1, SCD, SCEL, SH2D1B, SH3PXD2B, SIRPA, SIRPB1, SIRPG, SLAMF9, SLC2A6, SLC4A1, SLC9A7, SOCS3, SORT1, SPN, SYCP2, TLR7, TLR8, TMEM121B, TMSB4Y, TNF, TRAF1, TREML2

recurrence-free survival compared with other patients by analyzing a proteomic data set⁴³ (Figure 16C). These results suggest that PF4 is involved in the formation of the immunosuppressive microenvironment and the progression of HCC.

Discussion

Myeloid-lineage cells, especially intrahepatic macrophages, are central to NASH and HCC development.⁴ The action of intrahepatic macrophages involved in the pathogenesis of these diseases has been known to be secondary to external factors such as excessive nutrition, endotoxin influx, and hepatocyte damage, which induce macrophage differentiation and subsequent production of proinflammatory cytokines. Indeed, current animal models of NAFLD/NASH and HCC were generated mainly by applying nutrient-excessive or nutrient-deficient diet, chemical insults, spontaneous gene mutations, or gene-targeting to the whole body or liver parenchymal cells.^{44–46} In this study, we discovered for the first time that a myeloid-lineage-specific *Ncoa5* heterozygous deletion sufficiently causes insulin insensitivity, weight gain, NASH, and a moderate incidence of HCC in male mice fed a normal diet. These unexpected findings suggest that a genetic predisposition factor in myeloid-lineage cells can sufficiently induce the development of NAFLD, NASH, and HCC and highlight the importance of dysregulated myeloid cells that can promote the development of NAFLD, NASH, and HCC.

We focused on the *Ncoa5* ^{Δ M/+} mice in this study because *Ncoa5* ^{Δ M/ Δ M} mice exhibited less severe hepatic steatosis

compared with *Ncoa5* ^{Δ M/+} male mice and did not have increased body weight until 18 months old. The lessened effect of *Ncoa5*-null myeloid-lineage cells on the hepatocytes could be due to the impact of *Ncoa5* knockout on the cell proliferation or development, because *Ncoa5*-null RAW 264.7 cells were less proliferative than the vector control cells (Figure 17A and B). Nevertheless, elucidating why *Ncoa5* ^{Δ M/ Δ M} mice exhibited less severe hepatic steatosis requires further experimentation. Moreover, *Ncoa5* ^{Δ M/+} mice allow a more precise comparison with *Ncoa5*^{+/-} mice and better replicate the pathogenesis of humans containing heterozygous mutation or reduced cellular expression of NCOA5.

By combining cell-specific genetic and CRISPR/Cas9-knockout cells with transcriptomic studies, we found that before the advanced NASH in *Ncoa5* ^{Δ M/+} male mice, their intrahepatic macrophages had already exhibited a more M2-like phenotype in the intrahepatic macrophages rather than a proinflammatory phenotype that was often described as critical to their contribution to insulin resistance, hepatic steatosis, inflammation, and liver injury.^{47,48} The dysregulated pathways in these *Ncoa5* ^{Δ M/+} macrophages in the pre-NASH mouse livers were similar to those of obese humans who did not have a proinflammatory phenotype in their intrahepatic macrophages.²⁴ Moreover, the NCOA5- Δ M signature consisting of DEGs in *Ncoa5* ^{Δ M/+} intrahepatic macrophages can separate the NAFLD livers from the health control livers in the liver transcriptome data set. These results indicated that hepatic macrophages might promote the initiation and progression of hepatic steatosis through an

Figure 11. (See previous page). Comparison of transcriptome changes in intrahepatic macrophages between *Ncoa5* ^{Δ M/+} male mice and obese humans or NAFLD patients. (A) KEGG pathway analysis results comparing intrahepatic macrophages of *Ncoa5* ^{Δ M/+} vs *Ncoa5*^{fl/+} male mice ($n = 4$ each) (left) and obese humans ($n = 11$) vs non-obese humans ($n = 3$) (right) (PRJNA491664) using GAGE. Each dot represents a dysregulated KEGG pathway ($q < 0.1$). A red dot indicates that the same KEGG pathway is shared in both human and mouse analyses with the same direction in regulation. HM, intrahepatic macrophage. (B) The mRNA expression of PF4 and its non-allelic variant PF4V1 in intrahepatic macrophages from non-obese (nOB) and obese (OB) individuals. It was assessed by RNA-seq. P adjusted calculated by DESeq2. Box and whisker were drawn using the Tukey method drawing all data points. (C) ssGSEA enrichment scores of NCOA5- Δ M signature in liver transcriptomes of health control people ($n = 24$) and NAFLD patients (steatosis and NASH, $n = 39$) (GSE89632). Data represent mean \pm SEM. Two-tailed unpaired t test. (D) Correlations between NCOA5- Δ M enrichment z score and NAFLD clinical parameters, including ALT level, steatosis area, liver docosahexaenoic acid (DHA) level of total lipid, body mass index (BMI), triglyceride, waist length, aspartate transferase (AST), hemoglobin A1c (HbA1C), ballooning of hepatocyte, and liver arachidonic acid (AA) level of total lipid (GSE89632). Each dot represents 1 patient. Pearson's r and P values are indicated. * $P < .05$, ** $P < .01$, *** $P < .001$, **** $P < .0001$.

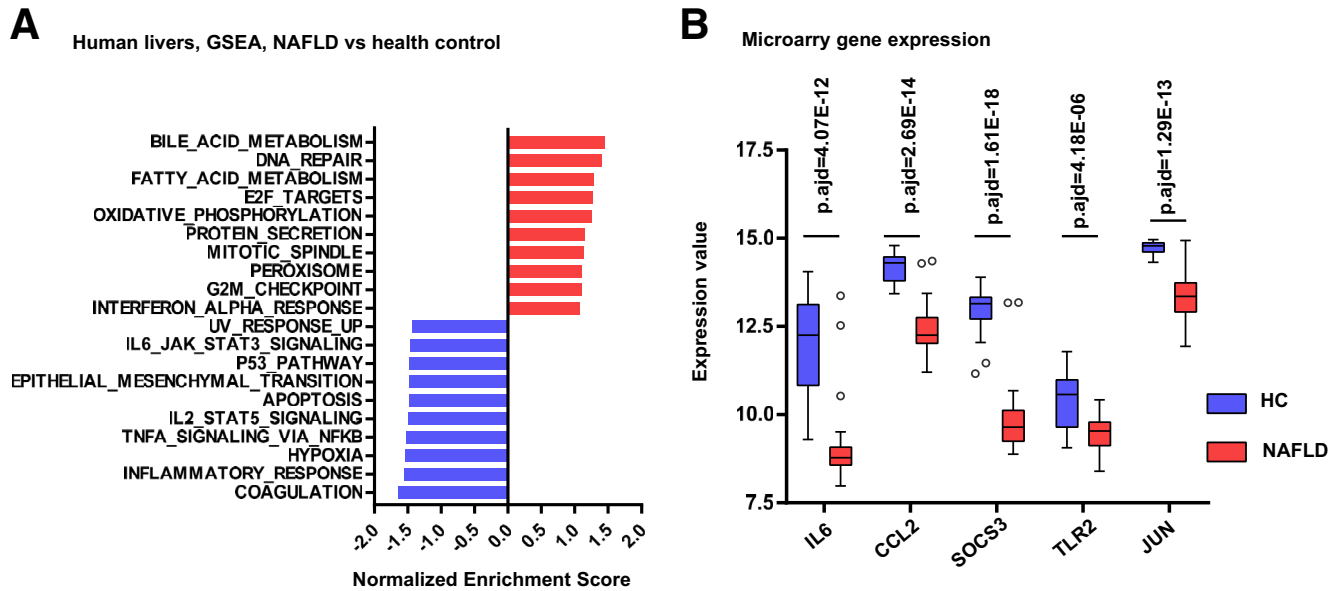


Figure 12. Expression of proinflammatory cytokines and signal pathways in NAFLD patients and healthy controls. (A) GSEA result of the hallmark gene set enrichment comparing the liver microarray data from health control people ($n = 24$) and NAFLD patients (steatosis and NASH, $n = 39$) (GSE89632). The top 10 positively and negatively enriched signatures in NAFLD patient samples compared with healthy control were shown. (B) Expression of selected inflammation-related genes from health control people ($n = 24$) and NAFLD patients (including patients with steatosis or NASH, $n = 39$) (GSE89632). Differential expression analysis with limma. Box and whisker were drawn using the Tukey method.

inflammation-independent pathway, which aligns with several recent studies.^{23,24}

Our findings raise the question of how NCOA5-deficient macrophages trigger the onset of hepatic steatosis. We hypothesize that NCOA5-deficient intrahepatic macrophages initiate hepatic steatosis, at least in part, by releasing excessive PF4. In support of this hypothesis, we found that *Pf4* was the most significantly up-regulated gene among the genes encoding secretory proteins in the intrahepatic macrophages of pre-NASH livers of *Ncoa5*^{ΔM/+} male mice and was continuously increased in the NASH livers of *Ncoa5*^{ΔM/+} male mice. Moreover, we observed that *Ncoa5*-null RAW 264.7 cells overexpressed PF4, and the conditional medium from these cells and recombinant PF4 protein directly stimulated lipid accumulation and lipogenic gene expression in hepatocytes. Our data from the experiment of in vivo knockdown of PF4 expression, specifically in intrahepatic macrophages, also indicate a critical role of PF4 secreted from intrahepatic macrophages in up-regulating lipogenic gene expression in livers of *Ncoa5*^{ΔM/+} male mice (Figure 10). Increased hepatic PF4 has been reported in the livers of rats fed a Westernized diet,⁴⁹ human alcoholic hepatitis patients,⁵⁰ and hepatitis C virus-infected patients with liver fibrosis.⁵¹ Although resident macrophages are known to express PF4,⁵² increased PF4 expression in macrophages has seldom been reported to be associated with NASH or NAFLD. Nevertheless, our studies found increased *Pf4* expression in the Kupffer cells of NASH livers in a published single-cell RNA-seq data set of an AMLN diet-induced mouse model of NASH.²¹ In addition, a study using a Westernized, sucrose/fructose-supplemented diet also

identified *Pf4* as a continuously up-regulated gene in intrahepatic macrophages of NAFLD mice.²⁰ Importantly, our results demonstrated that PF4 overexpression in intrahepatic macrophages was required for the up-regulation of lipogenic genes and lipid accumulation in this diet-induced mouse model of NAFLD (Figure 10).

PF4 was reported to interact with various receptors that mediate diverse signaling pathways in several cell types.⁵³ One of the receptors for PF4, CXCR3, is expressed in various liver cells, including hepatocytes, and has been shown to play a crucial role in obesity and NASH development by inducing actions including fatty acid synthesis.^{19,54} The functional binding of PF4 to CXCR3 has been well-established. The published evidence includes results of binding assay of radiolabeled PF4 to CXCR3 and using CXCR3 inhibitor (±)-AMG487, CXCR3-specific siRNA, and anti-CXCR3 antibodies to block the functional binding of PF4 to CXCR3.^{55,56} CXCR3 mediates multiple signaling pathways including PI3K/Akt and mTOR signaling, which could, in turn, alter the expression of lipogenic genes including *Pparg2*.^{16,57} Thus, the newly discovered pro-steatosis action of PF4 might be exerted by signaling the CXCR3 receptor. Nevertheless, our data do not rule out other mechanisms that also contribute to the development of insulin resistance and hepatic steatosis in *Ncoa5*^{ΔM/+} male mice initially. For example, another identified up-regulated gene in the intrahepatic macrophages of *Ncoa5*^{ΔM/+} male mice, *Angptl7* (Figure 17C), encodes a secreted protein that has been recently reported to promote insulin resistance and T2D.⁵⁸ Moreover, proinflammatory cytokines might contribute to the progression of simple hepatic steatosis to NASH and

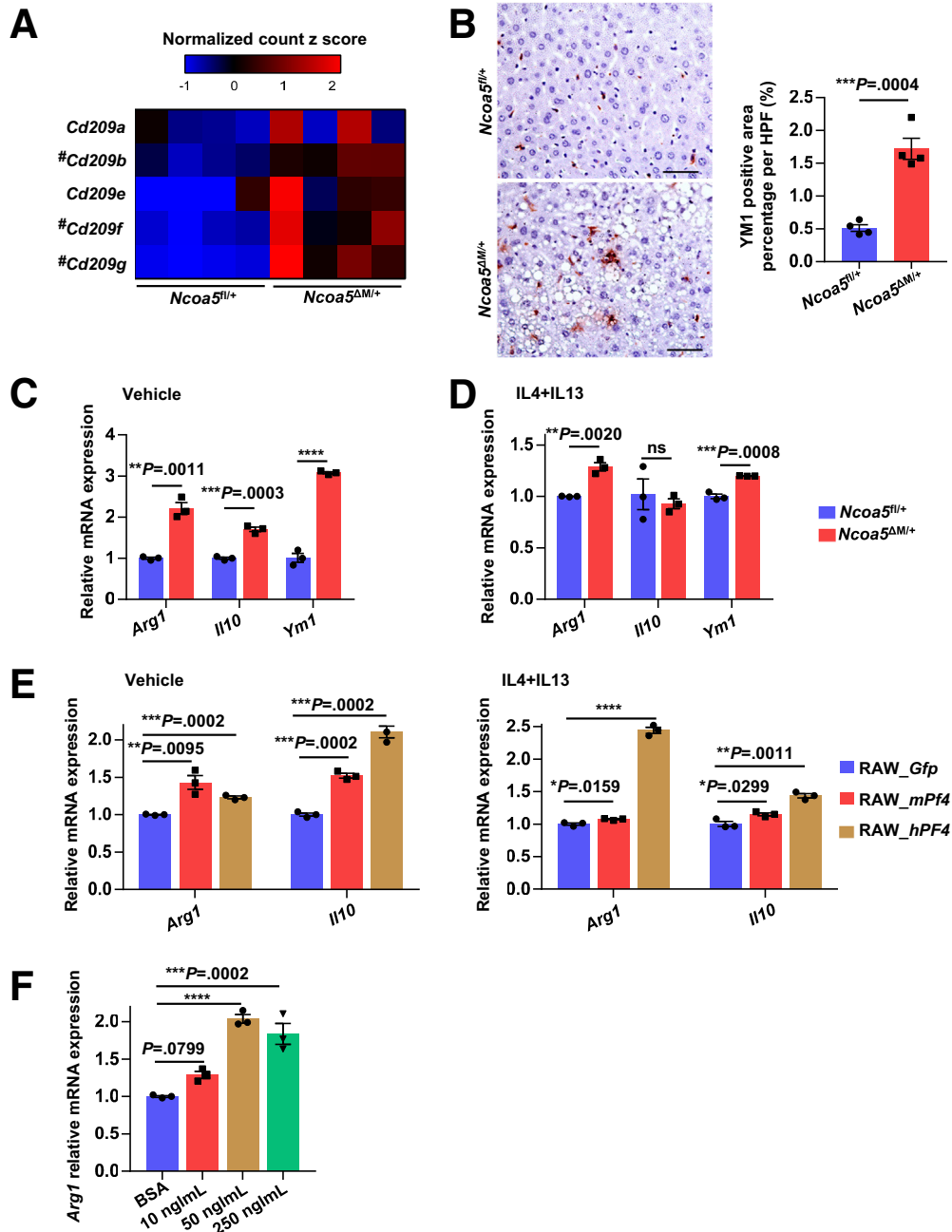


Figure 13. Effects of myeloid-lineage-specific *Ncoa5* heterozygous deletion on macrophage M2-like polarization. (A) Differences in mRNA expression of Cd209 family genes between intrahepatic macrophages from 6.5-month-old *Ncoa5^{fl/+}* ($n = 4$) and *Ncoa5^{ΔM/+}* ($n = 4$) male mice. Gene expression was visualized as z scores within each gene comparison using DESeq2 normalized counts. # represents adjusted P value $< .01$ reported by DESeq2 DEG analysis. (B) Representative photos of liver sections from 10-month-old *Ncoa5^{fl/+}* ($n = 4$) and *Ncoa5^{ΔM/+}* ($n = 4$) male mice and quantification of stained area positive for YM1 by IHC. 5 HPFs per mouse. (C and D) RT-qPCR analysis of mRNA expression of M2-macrophage markers in mouse peritoneal macrophages isolated from 6-week-old *Ncoa5^{fl/+}* and *Ncoa5^{ΔM/+}* male mice treated with vehicle (C) or mouse IL-4 and IL-13 (D). Pooled RNA from 2 or 3 mice in each group. (E) RT-qPCR analysis of mRNA levels of M2-macrophage markers in RAW 264.7 cells with ectopic PF4 expression treated with vehicle (left) or 20 ng/mL mouse IL-4 and IL-13 (right) for 24 hours. (F) RT-qPCR showing *Arg1* mRNA expression in RAW 264.7 cells treated with vehicle or mouse PF4 for 1 day. Representative data of 3 repeats. One-way analysis of variance Dunnett's multiple comparisons test. Data represent mean \pm SEM. Two-tailed unpaired t test was used if not otherwise specified. $*P < .05$, $**P < .01$, $***P < .001$, $****P < .0001$. Scale bar: 50 μ m.

HCC after the onset of fat accumulation in hepatocytes in *Ncoa5^{ΔM/+}* male mice. Regardless of whether other factors contributed to the pathogenesis of NAFLD in *Ncoa5^{ΔM/+}* male

mice, the finding that *Pf4* overexpression in intrahepatic macrophages can signal to hepatocytes and increase the expression of lipogenic genes is both significant and innovative.

The precise mechanism for the spontaneous HCC development in *Ncoa5*^{ΔM/+} male mice remains unclear. Although the links between NAFLD and HCC remain to be fully elucidated, previous data have suggested several underlying mechanisms.^{59,60} Because the immunosuppressive hepatic microenvironment is pivotal to the transition from NAFLD/NASH to HCC,⁶¹ it is conceivable that intrahepatic immunosuppressive immune cells contribute to hepatocarcinogenesis in *Ncoa5*^{ΔM/+} male mice having NASH. Consistent with this model, we found that *Ncoa5*^{ΔM/+} male mice had increased M2-like intrahepatic macrophages that transcriptomically differ from M0, M1, or M4 macrophages,^{62,63} and recombinant PF4 treatment or ectopic *Pf4* overexpression in RAW 264.7 cells could induce an M2-like phenotype. PF4 was reported to induce Treg proliferation while inhibiting nonregulatory T-cell proliferation³⁵ and promote breast tumor progression and metastasis by regulating MDSCs and inhibiting CD8+ T cells.³⁶ Interestingly, when we analyzed the TCGA HCC cohort for the association of tumor PF4 mRNA expression (possibly from tumor-associated macrophages) with patient survival or immunosuppressive cells, we not only found that high PF4 expression is associated with poor overall survival but also saw increased inferred M2 macrophage fractions. Moreover, enriched Treg and MDSC signatures in the tumor were associated with high PF4 expression. In line with our findings, the up-regulation of PF4 and its impact on cell proliferation and metastatic potential were also found in other solid tumors including pancreatic and lung cancers.⁶⁴ These data support the role of PF4 in HCC immunosuppression, and therefore, future work exploring the use of PF4 signaling inhibitors in HCC immunotherapy is warranted.

The relatively low HCC incidence in the NASH liver of *Ncoa5*^{ΔM/+} male mice compared with *Ncoa5*^{+/-} male mice suggests the contributions of other NCOA5-deficient cells, such as hepatocytes and pancreatic islet cells, to the higher HCC incidence in *Ncoa5*^{+/-} male mice. Nevertheless, NASH patients also have a moderate incidence and prolonged latency of human HCC, which *Ncoa5*^{ΔM/+} mice can model. We expect that additional genetic modification in the *Ncoa5*^{ΔM/+} mice or feeding them special diets can accelerate the NASH establishment and HCC development, enabling us to study further the mechanisms underlying NASH to HCC transition.

In summary, we established a novel genetic mouse model of NASH generated by myeloid-lineage-specific heterozygous deletion of *Ncoa5*, uncovering a molecular mechanism in which NCOA5 haploinsufficiency in myeloid cells triggers and propagates NASH development through PF4 overexpression in intrahepatic macrophages, leading to HCC development. *Ncoa5*^{ΔM/+} mice may provide a useful preclinical tool for NASH research. We anticipate that this work will lead to further insights into the pathogenesis of NASH to advance the future development of treatments for NASH and HCC.

Methods

Generation of *Ncoa5*^{fl/+}, *Ncoa5*^{fl/fl}, *Ncoa5*^{ΔM/+}, *Ncoa5*^{ΔM/ΔM}, and *Ncoa5*^{ΔH/ΔH} Mice

The *Ncoa5*^{fl/+} mice were generated by Cyagen (Santa Clara, CA). The targeting vector for LoxP site insertions

contains homology arms flanking exons 3 and 4 of the *Ncoa5* gene, LoxP sites, and *neo* gene flanked Rox sites. The correctly targeted C57BL/6 embryonic stem cell clones were confirmed by Southern blotting. Embryonic stem cells were then transfected with a Dre expression vector to remove the neomycin cassette. Correct clones were then subjected to blastocyst microinjection, and chimeras were produced. Crossbreeding the chimeras with wild-type C57BL/6 mice obtained founders that were transmitted in the germline. Genotyping for LoxP sites flanking the *Ncoa5* gene was performed using primers: forward: GATTCAGC-CAGGCAGTCCACAGAT; reverse: AATGGGCAAGAGTAGATGAGTTTCC. *Ncoa5*^{fllox/fllox} mice were generated by mating *Ncoa5*^{fllox/+} mice. LysMcre mice were purchased from the Jackson Laboratory. *Ncoa5*^{ΔM/+} mice were generated by crossing *Ncoa5*^{fllox/fllox} mice with heterozygote LysMcre mice. *Ncoa5*^{ΔM/ΔM} mice were first generated by mating *Ncoa5*^{ΔM/+} mice and then by crossing *Ncoa5*^{ΔM/ΔM} mice with *Ncoa5*^{fllox/fllox} mice. Genotyping for LysMcre was carried out using primers suggested by Jackson Laboratory. *Speer6-ps1*^{Alb-cre/+} mice were purchased from the Jackson Laboratory, and *Ncoa5*^{ΔH/ΔH} mice were generated using the same strategy as the *Ncoa5*^{ΔM/ΔM} mice. All mice except those wild-type C57BL/6 male mice enrolled for diet-induced NAFLD were housed in Optimice cages under a regular 12-hour light/12-hour dark cycle and standard normal diet at the Michigan State University animal facility. All experimental procedures on mice were approved by the Michigan State University Institutional Animal Care and Use Committee.

Glucose Tolerance Test and Insulin Tolerance Test

Glucose tolerance test (GTT) and insulin tolerance test (ITT) were performed as previously described.⁹ Briefly, mice were fasted for 12 or 6 hours before the intraperitoneal injection of 2 g/kg D(+)-glucose or 1 U/kg insulin (Sigma-Aldrich) for GTT or ITT. A glucometer and Accu-Check active test strips (Roche) were used to measure blood glucose from blood drops from the tail vein.

Western Blotting

Western blotting was performed as previously described.⁹ Generally, the protein was isolated using RIPA buffer (Thermo Fisher) from tissue or cell samples. Total protein concentration was measured by Biorad Protein Assay (Biorad), and sodium dodecyl sulfate-polyacrylamide gel electrophoresis was carried out on Biorad Mini-protein TGX Gels. LICOR IRDye secondary antibodies were used.

Antibodies and Recombinant Protein

Antibodies used in this study include β-Actin (sc-47778), p21 (sc-6246), and PPARγ (sc-7273) by Santa Cruz Biotechnology; Mac-2 (Galectin-3, CL8942AP) by Cedarlane Labs; NCOA5 (A300-790A) by Bethyl Laboratories; YM1 (AF-2446) by R&D Systems; PF4 (500-P05) by PeproTech; Akt (pan) (C67E7, #4691); and Phospho-Akt (Ser473) (#9271) by Cell Signaling Technology. Recombinant murine

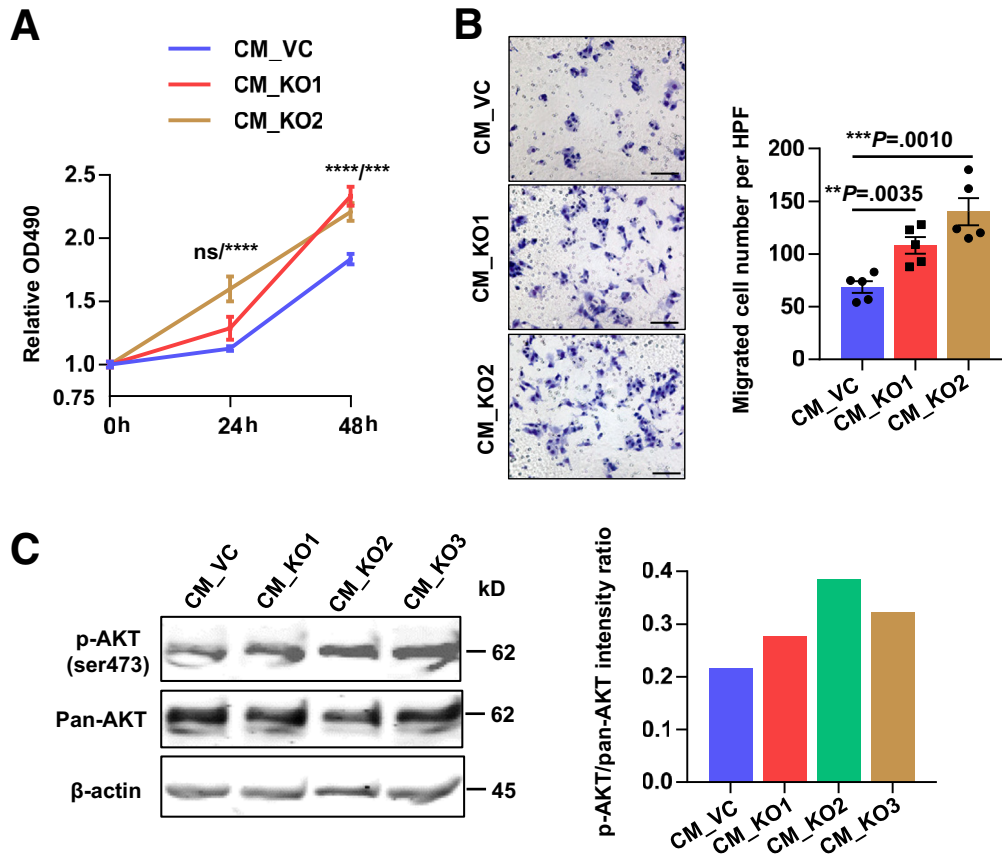


Figure 14. Effect of CM of *Ncoa5* knockout RAW 264.7 cells on proliferation and migration of HCC cells. (A) CCK8 assay of proliferation of HepG2 cells cultured with CM from RAW 264.7 cells with or without *Ncoa5* knockout with final concentration of 2% fetal bovine serum. Representative data of 2 repeats. Two-way analysis of variance Dunnett's multiple comparisons test. (B) Representative photos and quantification of migrated cells for HepG2 cell Transwell migration assay using CM from RAW 264.7 cells with or without *Ncoa5* knockout. 5 HPFs in each condition, representative result of 2 independent experiments. Two-tailed unpaired *t* test. (C) Western blotting analysis of AKT ser-473 phosphorylation in starved HepG2 cells treated with CM from RAW 264.7 cells with or without *Ncoa5* knockout. HepG2 cells were serum-starved for 24 hours and then treated with different CM for 20 minutes. Data in A and B represent mean \pm SEM. ***P* < .01, ****P* < .001, *****P* < .0001. Scale bar: 50 μ m.

PF-4 (250-39), murine IL-4 (214-14), and murine IL-13 (210-13) were purchased from PeproTech.

Histologic and Immunohistochemistry Analysis

Mouse tissues were fixed in neutrally buffered 10% formalin solution (Sigma-Aldrich). Fixed tissues were then submitted to the Investigative Histopathology Laboratory of Michigan State University for embedding, sectioning, and H&E staining. A board-certified pathologist reviewed the histopathology of mouse liver sections. Oil-Red-O staining and Sirius Red staining were performed according to published protocols.^{65,66} Immunohistochemistry analysis was performed using the VECTASTAIN ABC-HRP system (Vector Laboratories) according to the protocol supplied by the manufacturer.

Microscopic photos were captured using a Nikon ECLIPSE E600 microscope with a QImaging MicroPublisher 6 camera (Teledyne Photometrics). Macroscopic photo images were captured using a Nikon COOLPIX L340 camera.

RNA Preparation, Reverse Transcription, and RT-qPCR

Total RNA from mouse tissues, isolated cells, or cultured cells was isolated using TRIzol reagent (Thermo Fisher) or combined TRIzol and RNeasy Mini Kit (Qiagen) method according to manufacturers' instructions. Reverse transcription was performed using SuperScript IV First-Strand Synthesis System (Thermo Fisher) and PrimeScript RT Reagent Kit (TAKARA) according to manufacturers' instructions. RT-qPCR was carried out on a QuantStudio 3 Real-Time PCR machine using the PowerUp SYBR Green reagent (Thermo Fisher). Oligonucleotide sequences for the primers are described in Table 2.

Cell Culture, CRISPR, Gene Silencing, and Lentiviral Gene Expression

Mouse macrophage RAW 264.7 (derived from male) and human liver cancer cell line HepG2 (derived from male) were purchased from American Type Culture Collection and

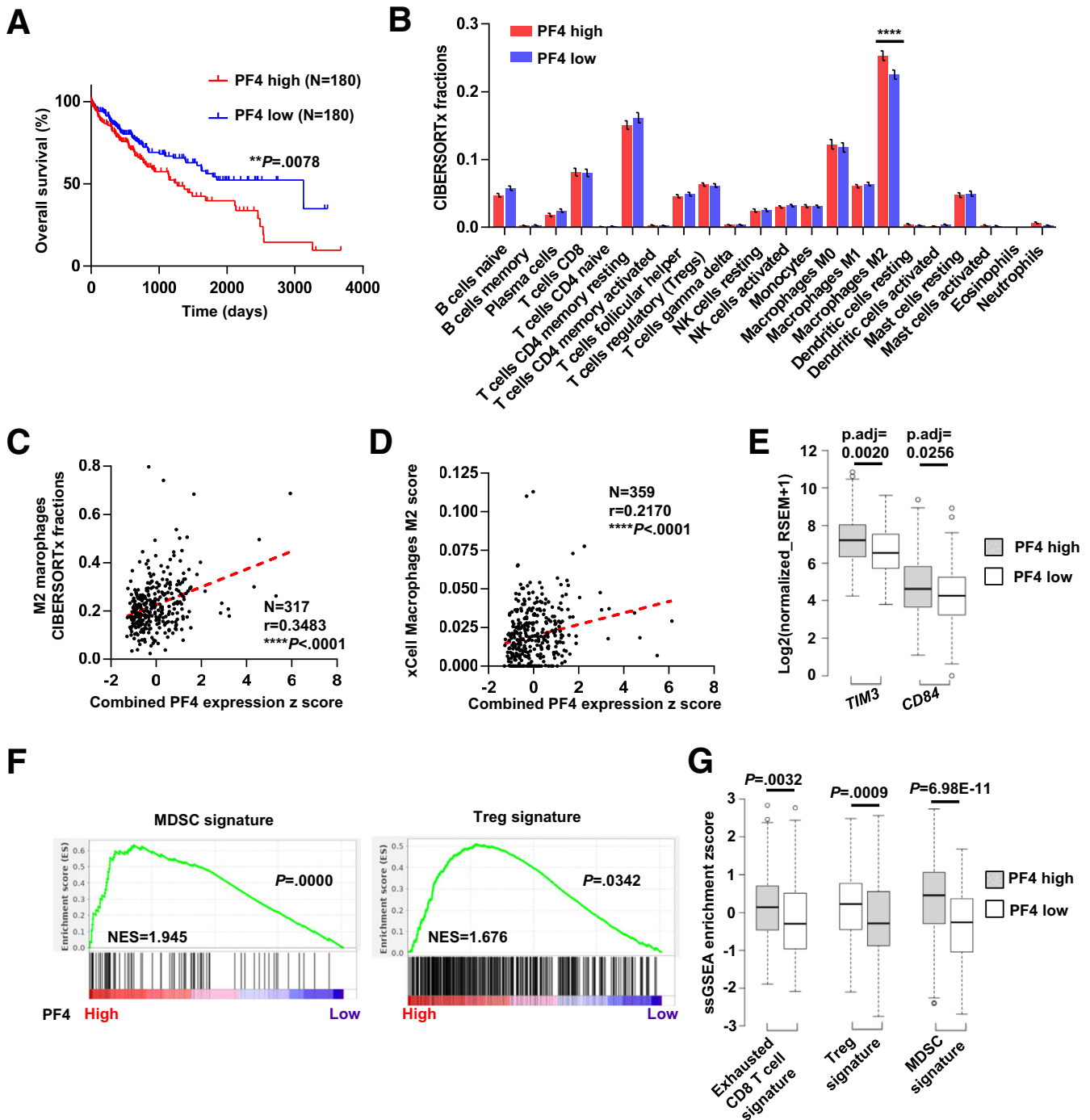


Figure 15. Relationships between PF4 expression in TCGA HCC patients and survival, M2 macrophage population, and immunosuppression-related gene signatures. (A) Kaplan Meier plot of overall survival for TCGA primary HCC patients with high ($n = 180$) or low ($n = 180$) combined PF4 and PF4V1 expression in the tumor (referred to as PF4 high or low groups in this and the next figure). Log-rank test. Combined PF4 and PF4V1 expression was ranked by ssGSEA. PF4 high group includes patients with top 50% of combined expression, and the low group includes the rest. ** $P < .01$. (B) Predicted immune cell fractions in HCCs of combined PF4 and PF4V1 high or low TCGA patients by CIBERSORTx absolute mode. Samples with $P > .05$ were filtered. Patients, $n = 165$ and 152. Two-way analysis of variance Sidak's multiple comparison test was used for statistical analysis. Data represent mean \pm SEM. **** $P < .0001$. (C) Correlation between combined tumoral PF4 and PF4V1 expression and predicted M2 macrophage fractions in TCGA patients. Pearson's r and P values and patient numbers are indicated. Patient separation was done in (B) and (C) as described in (A), except 43 patient samples were filtered because of their CIBERSORTx $P > .05$. (D) Correlation between combined tumoral PF4 and PF4V1 expression and xCell Macrophages M2 score in TCGA patients. Pearson's r and P values and patient numbers are indicated. The same patient cohort as in (A–C) was used, but data for 2 patients were missing in the original xCell analysis performed by the authors of the tool. (E) Expression of immunosuppression-related genes in HCCs from TCGA patients with high or low combined PF4 and PF4V1 expression. Welch's t test with the FDR method of Benjamini-Hochberg. (F) GSEA analysis result using indicated signatures comparing HCCs from TCGA patients with high or low combined PF4 and PF4V1 expression. Normalized enrichment scores and P values are shown. (G) ssGSEA result of published gene sets as indicated in TCGA patients with high or low PF4 and PF4V1 mRNA expression. Two-tailed unpaired t test was used for statistical analysis. Box and whisker are drawn using the Tukey method.

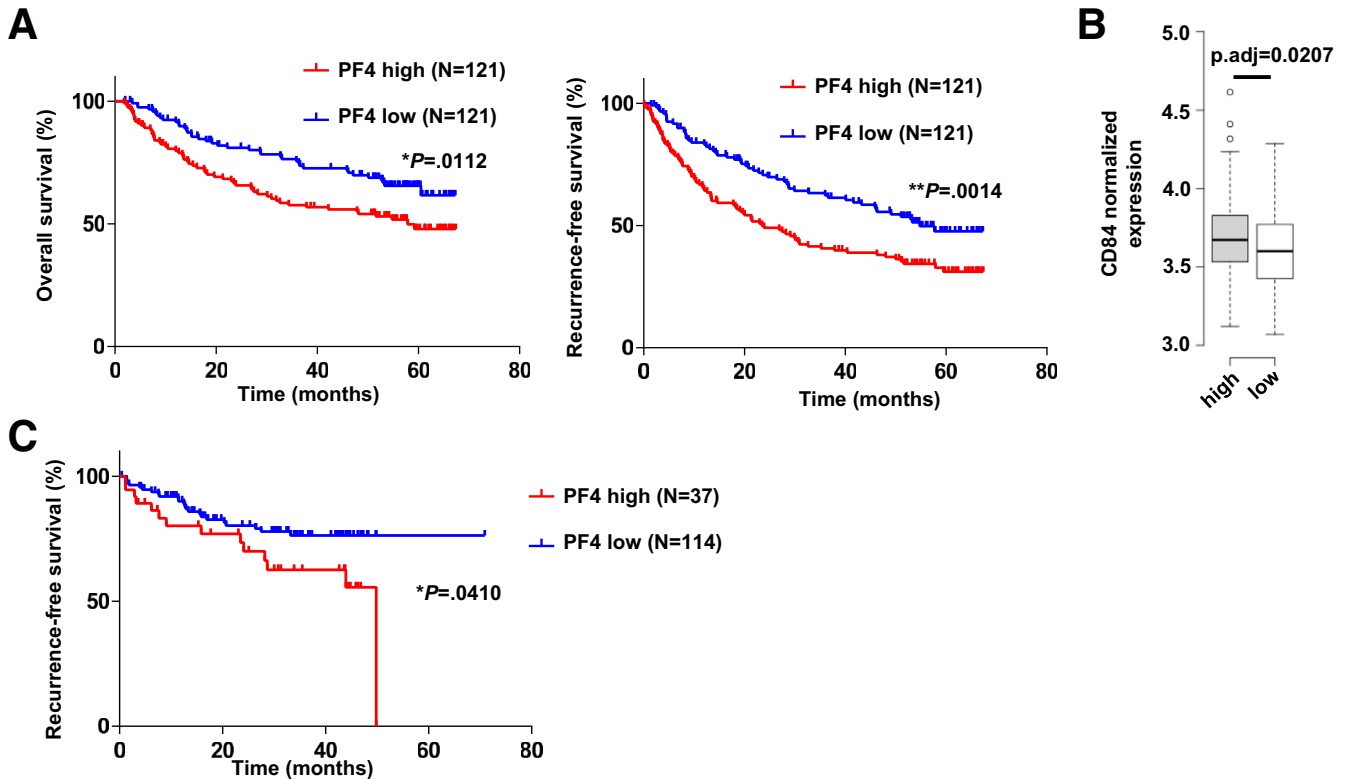


Figure 16. Relationships between tumoral PF4 expression and HCC patient prognosis in the LCI and proteomic study cohorts. (A) Kaplan-Meier plot of overall survival and recurrence-free survival for LCI primary HCC patients with high ($n = 121$) or low ($n = 121$) combined PF4 and PF4V1 expression in the tumor. Log-rank test. * $P < .05$, ** $P < .01$. (B) Expression of CD84 in HCCs from LCI patients with high or low PF4 expression. P adjusted calculated using limma. Box and whisker are drawn using the Tukey method. (C) Kaplan-Meier plot of recurrence-free survival for PDC000198 primary HCC patients with PF4 protein expression in the top quartile and the rest of patients. Log-rank test. * $P < .05$.

cultured in Dulbecco modified Eagle medium (DMEM) (Thermo Fisher) supplemented with 10% fetal bovine serum and 100 U/mL of penicillin and 100 $\mu\text{g}/\text{mL}$ of streptomycin at 37°C in 5% CO₂. For the collection of CM, 4×10^6 RAW 264.7 cells were plated in a 100 mm plate and cultured in serum-free DMEM for 24 hours. The medium was collected and centrifuged to remove cells and debris. The CM was centrifuged and mixed with the complete medium in a 1:1 ratio when treating cells with a CM.

CRISPR knockout of *Ncoa5* gene was achieved using pSpCas9(BB)-2A-Puro (PX459) V2.0 plasmid purchased from Addgene,⁶⁷ and the guide target sequences are the following: target1 (exon 3): CTGCGGTCCCGCAAATCCCG; target2 (exon 3): and CGTGATCGCTCTCCAATTCG; target3 (exon 4): ATATGACCGTTATCTGAGGG. The target sequences and PAMs were cloned into the PX459 V2.0 plasmid according to the target sequence cloning protocol described on Addgene. RAW 264.7 cells were transiently transfected with vector control or constructs using Lipofectamine 3000 (Thermo Fisher) and selected with 5 $\mu\text{g}/\text{mL}$ puromycin. Single clones were picked and cultured. Genomic DNA was extracted with QuickExtract (Lucigen), and PCR amplification and sequencing validation was performed. Finally, Western blotting was performed to validate the loss of NCOA5 protein.

RNA-induced gene silencing was performed using DsiRNAs purchased from Integrated DNA Technologies

according to the protocol supplied by the manufacturer. The siRNA sequences are the following: mm. Ri.Pf4.13.1-SEQ1/2: rGrGrGrCrArGrGrCrArGrUrGrArArGrArUrArArArCrGTG/rCrArCrGrUrUrUrUrArUrCrUrUrCrArCrUrGrCrCrUrGrCrCrArG; mm.Ri.Pf4.13.2-SEQ1/2: rCrCrGrArUrGrUrUrArUrArUrArUrCrUrUrCrArAGA/rUrCrUrUrGrArArGrGrArUrArArUrArUrArArArCrArUrCrGrGrArA.

The double-stranded DNA fragments of consensus coding sequences of mouse and human *Pf4* genes (CCDS 19416.1 and 3562.1) were synthesized by Integrated DNA Technologies and were cloned into the pSin-EF2-Pur vector (Addgene). Lentivirus was produced by polyethyleneimine-mediated transfection of HEK293T (ATCC) cells with pCMV delta R8.2 packaging plasmid (Addgene), pMD2.G envelope plasmid (Addgene), and pSin-EF2-PF4-Pur expression plasmid.

Mouse Liver Hepatocyte, Nonparenchymal Cell, F4/80+ Nonparenchymal Cell, and Peritoneal Macrophage Isolation

Primary hepatocytes were isolated from wild-type male mice and cultured according to a published protocol⁶⁸ with the following modifications: the portal vein was cannulated instead of the inferior vena cava, and the inferior vena cava was cut after the initial perfusion; plates/wells were prepared with 0.01% w/v rat-tail collagen (Sigma-Aldrich). Liver

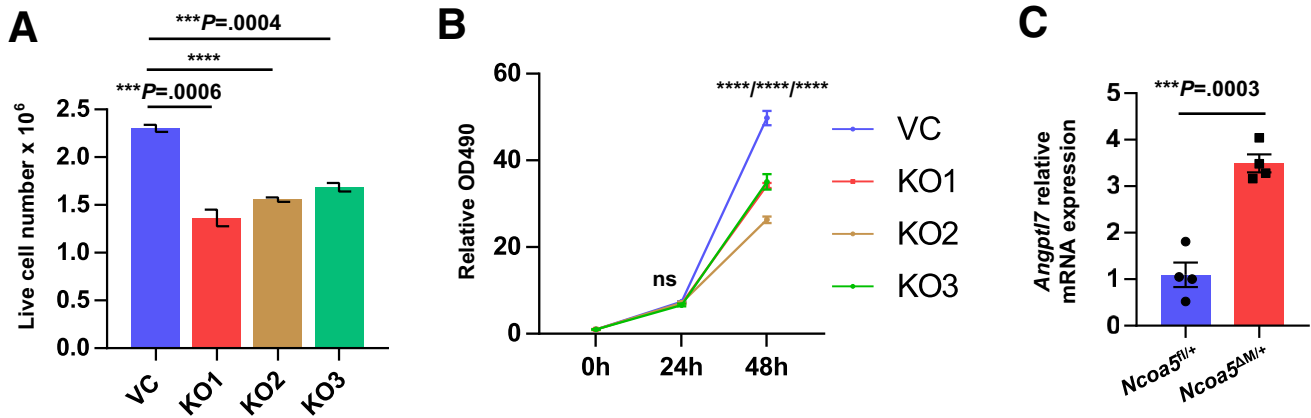


Figure 17. Role of NCOA5 in macrophage proliferation and *Angptl7* expression. (A) Live cell number of same initial amount of RAW 264.7 cells with or without *Ncoa5* knockout after 48-hour culture. Representative data of 3 repeats. Data represent mean \pm SEM. Two-tailed unpaired *t* test was used for statistical analysis. (B) CCK8 assay of proliferation of RAW 264.7 cells with or without *Ncoa5* knockout. Representative data of 3 repeats. Data represent mean \pm SEM. Two-way analysis of variance Dunnett's multiple comparisons test was used for statistical analysis. (C) The mRNA expression of *Angptl7* in intrahepatic macrophages from 6.5-month-old *Ncoa5*^{fl/+} and *Ncoa5*^{ΔM/+} male mice tested by RT-qPCR. Two-tailed unpaired *t* test. Data represent mean \pm SEM. ns: not significant, ****P* < .001, *****P* < .0001.

nonparenchymal cells were isolated in a 2-step perfusion procedure similar to the isolation of mouse hepatocytes. The F4/80+ cells were isolated from nonparenchymal cells using Anti-F4/80 MicroBeads (130-110-443, Miltenyi Biotec) according to the manufacturer's instructions. Peritoneal macrophages were isolated using ice-cold phosphate-buffered saline containing 3% fetal bovine serum from indicated mice.

RNA-Sequencing and Mouse Transcriptome Analysis

High-quality RNA was prepared from F4/80+ nonparenchymal cells using a combined TRIzol and RNeasy Mini Kit (Qiagen) method. RNA quality control was performed using the Nanodrop Spectrophotometer (Thermo Fisher) and TapeStation System (Agilent). cDNA library construction from mRNA, RNA-seq on a NovaSeq 6000 (Illumina), raw data quality control, and data delivery were carried out by Novogene. Approximately 90 million reads were generated for each sample. The raw data were filtered and quality-controlled using fastp.⁶⁹ The data quantification was performed using Salmon,⁷⁰ with the mapping-based mode and a salmon index built using Gencode mouse release M25 (GRCm38.p6). The gene expression analysis was performed using DESeq2.⁷¹ KEGG pathway analysis was carried out using GAGE.²⁵

Transcriptomic and Proteomic Analyses of Human Samples

RNA-seq raw data of human liver macrophages were downloaded from NCBI Sequence Read Archive PRJNA491664.²⁴ The data analysis procedure was the same as the mouse F4/80+ cells analysis, except that the reads were mapped using STAR,⁷² where higher mapping rates were achieved in this instance. The STAR index was built using Gencode human release 35 (GRCh38.p13). Human liver microarray data of NAFLD patients and healthy controls were downloaded from

NCBI Gene Expression Omnibus (GSE89632).²⁶ Processed expression and clinical data of patients in the TCGA LIHC cohort were retrieved from UCSC Xena. Processed microarray expression and clinical data of the LCI HCC cohort were downloaded from NCBI Gene Expression Omnibus (GSE14520).⁴² Gene expression difference between TCGA LIHC patient subgroups was determined with cBioportal.⁷³ Differential expression analysis for microarray data was performed using limma.⁷⁴ Gene set enrichment analysis (GSEA) version 4.2.1 and ssGSEA v10 were used,^{27,41} and the analysis was carried out on GenePattern. CIBERSORTx was run in absolute mode according to the published instructions.^{75,76} xCell cell types enrichment analysis for TCGA patients was pre-calculated by the authors of xCell and retrieved from the xCell website.³⁸

Processed protein quantitation and clinical data from a published HCC proteogenomic study were downloaded from the NIH Proteomic Data Commons (PDC000198).⁴³

In the TCGA LIHC cohort, 12% of patients had low NCOA5 mRNA expression ($z < -1$ relative to diploid samples), and 3.6% had NCOA5 shallow deletion, missense mutation, or truncating mutation in their tumors.

Single-Cell Transcriptomic Analysis of Diet-Induced NASH Mouse Livers

Single-cell sequencing raw data of nonparenchymal cells from healthy and diet-induced NASH mouse livers were downloaded from NCBI Sequence Read Archive PRJNA531644. The data analysis procedure was the same as in the original publication.²¹ Our analysis revealed 10 major cell clusters similar to the original publication (Figure 7A).

Intrahepatic-Macrophage-Specific Gene Knockdown Mediated By GeRP

GeRPs were prepared according to published protocols,²²⁻²⁴ with the modification of no fluorescein

Table 2. Oligos Used in the Study

Genes	Forward	Reverse
Polr2a	GCGGTTGACCCCATGACGAGTGAT	GCCTGATGCGGGTGCTGAGTGAG
Srebp1c	GGAGCCATGGATTGCACATT	GGCCCGGAAGTCACTGT
ChREBP/Mlxipl	AATGGGATGGTGTCTACCGC	GGCGAAGGGAATTCAGGACA
Pparg1	TGAAAGAAGCGGTGAACCACTG	TGGCATCTCTGTGTCAACCATG
Pparg2	GCATGGTGCCCTTCGCTGA	TGGCATCTCTGTGTCAACCATG
G6pc	TGGTAGCCCTGTCTTTCTTTG	TTCCAGCATTACACTTTTCT
Fasn	CCTCAAGGCTGCGTAGACAC	GCCACATCATGCTGCTGCAGT
Acaca/Acc	GTCCCCAGGGATGAACCAATA	GCCATGCTCAACCAAAGTAGC
Plin2/Adrp	AAGAGAAGCATCGGCTACGA	GGCGATAGCCAGAGTACGTG
Cd36	GATGACGTGGCAAAGAACAG	TCCTCGGGTCTGAGTTAT
Cidec/Fsp27	AGGCCCTGTGTTAGCAC	CATGATGCCTTTGCGAACCT
p21/Cdkn1a	CAGATCCACAGCGATATCC	ACGGGACCGAAGAGACAAC
Pf4	TGCACTTAAGAGCCCTAGACCCAT	AGATCTCCATCGCTTTCTTCGGGA
Tnf	GCCTATGTCTCAGCCTCTTCT	TTGAGATCCATGCCGTTGGCC
Cxcr3	CAGCCTGAACTTTGACAGAACCT	GCAGCCCCAGCAAGAAGA
Gas6	TGCTGGCTTCCGAGTCTTC	CGGGGTCGTTCTCGAACAC
Arg1	CTTGCGAGACGTAGACCCTG	TCCATCACCTTGCCAATCCC
Ym1	GTACCCTGGGTCTCGAGGAA	CCTTGAATGTCTTTCTCCACAG
Il10	CCAGGGAGATCCTTTGATGA	AACTGGCCACAGTTTTCAGG

isothiocyanate labeling steps. Wild-type C57BL/6 male mice were fed with a Westernized and sucrose/fructose supplemented diet (D09061704i, Research Diets, Inc) starting at 6 weeks of age for 3 months to induce NAFLD with a concurrent *Pf4* up-regulation specifically in hepatic macrophages.²⁰ GeRP administration was carried out according to published articles with slight modifications.^{23,24} Mice fed the special diet were randomized according to body weight and intravenously injected with a dose of 6.25 mg/kg GeRPs loaded with 247 $\mu\text{g}/\text{kg}$ siRNA and 1.135 mg/kg Endo-Porter (EP, Gene Tools, LLC). Mice were switched to a normal diet 24 hours after GeRP administration, and samples were collected 1 week after GeRP administration. Seven-month-old *Ncoa5*^{ΔM/+} male mice fed a normal diet were randomized according to body weight and intravenously injected with 7 doses of 3.125 mg/kg GeRPs loaded with 123.5 $\mu\text{g}/\text{kg}$ siRNA and 0.5675 mg/kg EP over 2 weeks, and samples were collected 24 hours after the last injection. The siRNAs used in this study are proprietary Dharmacon D-001810-01-50 ON-TARGETplus Nontargeting siRNA #1 and J-063518-11-0050 ON-TARGETplus Mouse Pf4 (56744) siRNA (Horizon Discovery). The LQ-063518-01-0002 ON-TARGETplus Mouse Pf4 (56744) siRNA set of 4 was initially tested, and the siRNA with the highest efficiency was identified and used in formal experiments.

Cell Proliferation and Colorimetric Assays

The 1×10^5 RAW 264.7 cells were seeded in 12-well plates and cultured 48 hours in the DMEM complete medium. Cell numbers were then counted using a Countess II FL hemocytometer with an automated cell counter (Thermo Fisher). For the colorimetric cell proliferation assay, 1500 RAW 264.7 cells or 4000 HepG2 cells were seeded in

96-well plates, and CCK-8 (Dojindo) was used to determine the cell number according to the protocol supplied by the manufacturer. Triglyceride levels in liver homogenates and cell lysates were measured using Triglyceride Colorimetric Assay Kit (Cayman Chemical) according to the protocol provided by the manufacturer. Absorbance was read by a FLUOstar OPTIMA microplate reader (BMG LABTECH).

Transwell Migration Assay

Transwell permeable assay (Ref 3422, Costar) plated with 1×10^5 HepG2 cells in serum-free DMEM was inserted into a 24-well plate containing medium conditioned by RAW 264.7 cells mixed with DMEM with 2.5% fetal bovine serum. After 24 hours, the membranes were stained with Giemsa stain (Sigma-Aldrich).

Statistical Analyses

All data represent \pm standard error of the mean (SEM) from the mean if not otherwise specified. Statistical differences were determined with one-way analysis of variance Dunnett's multiple comparisons test, two-way analysis of variance Dunnett's multiple comparisons test and Sidak's multiple comparisons test, two-tailed Student *t* test, Welch's *t* test, χ^2 test, Pearson's correlation two-tailed significance test, or log-rank test by GraphPad Prism 7, with details listed in the corresponding figure legends. *****P* < .0001, ****P* < .001, ***P* < .01, **P* < .05, ns = not significant.

References

- Cotter TG, Rinella M. Nonalcoholic fatty liver disease 2020: the state of the disease. *Gastroenterology* 2020; 158:1851–1864.

2. Anstee QM, Day CP. The genetics of nonalcoholic fatty liver disease: spotlight on PNPLA3 and TM6SF2. *Semin Liver Dis* 2015;35:270–290.
3. Friedman SL, Neuschwander-Tetri BA, Rinella M, et al. Mechanisms of NAFLD development and therapeutic strategies. *Nat Med* 2018;24:908–922.
4. Kazankov K, Jorgensen SMD, Thomsen KL, et al. The role of macrophages in nonalcoholic fatty liver disease and nonalcoholic steatohepatitis. *Nat Rev Gastroenterol Hepatol* 2019;16:145–159.
5. Gillespie MA, Gold ES, Ramsey SA, et al. An LXR-NCOA5 gene regulatory complex directs inflammatory crosstalk-dependent repression of macrophage cholesterol efflux. *EMBO J* 2015;34:1244–1258.
6. Jiang C, Ito M, Piening V, et al. TIP30 interacts with an estrogen receptor alpha-interacting coactivator CIA and regulates c-myc transcription. *J Biol Chem* 2004;279:27781–27789.
7. Sauve F, McBroom LD, Gallant J, et al. CIA, a novel estrogen receptor coactivator with a bifunctional nuclear receptor interacting determinant. *Mol Cell Biol* 2001;21:343–353.
8. Lewis JP, Palmer ND, Ellington JB, et al. Analysis of candidate genes on chromosome 20q12–13.1 reveals evidence for BMI mediated association of PREX1 with type 2 diabetes in European Americans. *Genomics* 2010;96:211–219.
9. Gao S, Li A, Liu F, et al. NCOA5 haploinsufficiency results in glucose intolerance and subsequent hepatocellular carcinoma. *Cancer Cell* 2013;24:725–737.
10. Williams M, Liu X, Zhang Y, et al. NCOA5 deficiency promotes a unique liver protumorigenic microenvironment through p21(WAF1/CIP1) overexpression, which is reversed by metformin. *Oncogene* 2020;39:3821–3836.
11. Abram CL, Roberge GL, Hu Y, et al. Comparative analysis of the efficiency and specificity of myeloid-Cre deleting strains using ROSA-EYFP reporter mice. *J Immunol Methods* 2014;408:89–100.
12. Itoh M, Kato H, Suganami T, et al. Hepatic crown-like structure: a unique histological feature in non-alcoholic steatohepatitis in mice and humans. *PLoS One* 2013;8:e82163.
13. Benhamed F, Denechaud PD, Lemoine M, et al. The lipogenic transcription factor ChREBP dissociates hepatic steatosis from insulin resistance in mice and humans. *J Clin Invest* 2012;122:2176–2194.
14. Foretz M, Guichard C, Ferre P, et al. Sterol regulatory element binding protein-1c is a major mediator of insulin action on the hepatic expression of glucokinase and lipogenesis-related genes. *Proc Natl Acad Sci U S A* 1999;96:12737–12742.
15. Knebel B, Haas J, Hartwig S, et al. Liver-specific expression of transcriptionally active SREBP-1c is associated with fatty liver and increased visceral fat mass. *PLoS One* 2012;7:e31812.
16. Lee YK, Park JE, Lee M, et al. Hepatic lipid homeostasis by peroxisome proliferator-activated receptor gamma 2. *Liver Res* 2018;2:209–215.
17. Naugler WE, Sakurai T, Kim S, et al. Gender disparity in liver cancer due to sex differences in MyD88-dependent IL-6 production. *Science* 2007;317:121–124.
18. Schmidt-Arras D, Rose-John S. IL-6 pathway in the liver: from physiopathology to therapy. *J Hepatol* 2016;64:1403–1415.
19. Zhang X, Han J, Man K, et al. CXC chemokine receptor 3 promotes steatohepatitis in mice through mediating inflammatory cytokines, macrophages and autophagy. *J Hepatol* 2016;64:160–170.
20. Remmerie A, Martens L, Thone T, et al. Osteopontin expression identifies a subset of recruited macrophages distinct from Kupffer cells in the fatty liver. *Immunity* 2020;53:641–657 e14.
21. Xiong X, Kuang H, Ansari S, et al. Landscape of intercellular crosstalk in healthy and NASH liver revealed by single-cell secretome gene analysis. *Mol Cell* 2019;75:644–660 e5.
22. Barreby E, Sulen A, Aouadi M. Glucan-encapsulated siRNA particles (GeRPs) for specific gene silencing in adipose tissue macrophages. *Methods Mol Biol* 2019;1951:49–57.
23. Azzimato V, Jager J, Chen P, et al. Liver macrophages inhibit the endogenous antioxidant response in obesity-associated insulin resistance. *Sci Transl Med* 2020;12.
24. Morgantini C, Jager J, Li X, et al. Liver macrophages regulate systemic metabolism through non-inflammatory factors. *Nat Metab* 2019;1:445–459.
25. Luo W, Friedman MS, Shedden K, et al. GAGE: generally applicable gene set enrichment for pathway analysis. *BMC Bioinformatics* 2009;10:161.
26. Arendt BM, Comelli EM, Ma DW, et al. Altered hepatic gene expression in nonalcoholic fatty liver disease is associated with lower hepatic n-3 and n-6 polyunsaturated fatty acids. *Hepatology* 2015;61:1565–1578.
27. Barbie DA, Tamayo P, Boehm JS, et al. Systematic RNA interference reveals that oncogenic KRAS-driven cancers require TBK1. *Nature* 2009;462:108–112.
28. Rigamonti E, Chinetti-Gbaguidi G, Staels B. Regulation of macrophage functions by PPAR-alpha, PPAR-gamma, and LXRs in mice and men. *Arterioscler Thromb Vasc Biol* 2008;28:1050–1059.
29. Scheuerer B, Ernst M, Durrbaum-Landmann I, et al. The CXC-chemokine platelet factor 4 promotes monocyte survival and induces monocyte differentiation into macrophages. *Blood* 2000;95:1158–1166.
30. Drescher HK, Brandt EF, Fischer P, et al. Platelet factor 4 attenuates experimental acute liver injury in mice. *Front Physiol* 2019;10:326.
31. Gleissner CA. Macrophage phenotype modulation by CXCL4 in atherosclerosis. *Front Physiol* 2012;3:1.
32. Pan Y, Yu Y, Wang X, et al. Tumor-associated macrophages in tumor immunity. *Front Immunol* 2020;11:583084.
33. Lin Y, Xu J, Lan H. Tumor-associated macrophages in tumor metastasis: biological roles and clinical therapeutic applications. *J Hematol Oncol* 2019;12:76.
34. Fleischer J, Grage-Griebenow E, Kasper B, et al. Platelet factor 4 inhibits proliferation and cytokine release of activated human T cells. *J Immunol* 2002;169:770–777.
35. Liu CY, Battaglia M, Lee SH, et al. Platelet factor 4 differentially modulates CD4+CD25+ (regulatory) versus CD4+CD25- (nonregulatory) T cells. *J Immunol* 2005;174:2680–2686.

36. Joseph R, Soundararajan R, Vasaikar S, et al. CD8(+) T cells inhibit metastasis and CXCL4 regulates its function. *Br J Cancer* 2021;125:176–189.
37. Newman AM, Steen CB, Liu CL, et al. Determining cell type abundance and expression from bulk tissues with digital cytometry. *Nat Biotechnol* 2019;37:773–782.
38. Aran D, Hu Z, Butte AJ. xCell: digitally portraying the tissue cellular heterogeneity landscape. *Genome Biol* 2017;18:220.
39. Alshetaiwi H, Pervolarakis N, McIntyre LL, et al. Defining the emergence of myeloid-derived suppressor cells in breast cancer using single-cell transcriptomics. *Sci Immunol* 2020;5.
40. Zheng C, Zheng L, Yoo JK, et al. Landscape of infiltrating T cells in liver cancer revealed by single-cell sequencing. *Cell* 2017;169:1342–1356 e16.
41. Subramanian A, Tamayo P, Mootha VK, et al. Gene set enrichment analysis: a knowledge-based approach for interpreting genome-wide expression profiles. *Proc Natl Acad Sci U S A* 2005;102:15545–15550.
42. Roessler S, Jia HL, Budhu A, et al. A unique metastasis gene signature enables prediction of tumor relapse in early-stage hepatocellular carcinoma patients. *Cancer Res* 2010;70:10202–10212.
43. Gao Q, Zhu H, Dong L, et al. Integrated proteogenomic characterization of HBV-related hepatocellular carcinoma. *Cell* 2019;179:561–577 e22.
44. Hansen HH, Feigh M, Veidal SS, et al. Mouse models of nonalcoholic steatohepatitis in preclinical drug development. *Drug Discov Today* 2017;22:1707–1718.
45. Farrell G, Schattenberg JM, Leclercq I, et al. Mouse models of nonalcoholic steatohepatitis: toward optimization of their relevance to human nonalcoholic steatohepatitis. *Hepatology* 2019;69:2241–2257.
46. Zhong F, Zhou X, Xu J, et al. Rodent models of nonalcoholic fatty liver disease. *Digestion* 2020;101:522–535.
47. Carter-Kent C, Zein NN, Feldstein AE. Cytokines in the pathogenesis of fatty liver and disease progression to steatohepatitis: implications for treatment. *Am J Gastroenterol* 2008;103:1036–1042.
48. Fuentes L, Roszer T, Ricote M. Inflammatory mediators and insulin resistance in obesity: role of nuclear receptor signaling in macrophages. *Mediators Inflamm* 2010;2010:219583.
49. Roberts MD, Mobley CB, Toedebush RG, et al. Western diet-induced hepatic steatosis and alterations in the liver transcriptome in adult Brown-Norway rats. *BMC Gastroenterol* 2015;15:151.
50. Dominguez M, Miquel R, Colmenero J, et al. Hepatic expression of CXC chemokines predicts portal hypertension and survival in patients with alcoholic hepatitis. *Gastroenterology* 2009;136:1639–1650.
51. Zaldivar MM, Pauels K, von Hundelshausen P, et al. CXC chemokine ligand 4 (Cxcl4) is a platelet-derived mediator of experimental liver fibrosis. *Hepatology* 2010;51:1345–1353.
52. Pertuy F, Aguilar A, Strassel C, et al. Broader expression of the mouse platelet factor 4-cre transgene beyond the megakaryocyte lineage. *J Thromb Haemost* 2015;13:115–125.
53. Gray AL, Karlsson R, Roberts ARE, et al. Chemokine CXCL4 interactions with extracellular matrix proteoglycans mediate widespread immune cell recruitment independent of chemokine receptors. *Cell Rep* 2023;42:111930.
54. Deiliulis JA, Oghumu S, Duggineni D, et al. CXCR3 modulates obesity-induced visceral adipose inflammation and systemic insulin resistance. *Obesity (Silver Spring)* 2014;22:1264–1274.
55. Lasagni L, Francalanci M, Annunziato F, et al. An alternatively spliced variant of CXCR3 mediates the inhibition of endothelial cell growth induced by IP-10, Mig, and I-TAC, and acts as functional receptor for platelet factor 4. *J Exp Med* 2003;197:1537–1549.
56. Tan S, Li S, Min Y, et al. Platelet factor 4 enhances CD4(+) T effector memory cell responses via Akt-PGC1alpha-TFAM signaling-mediated mitochondrial biogenesis. *J Thromb Haemost* 2020;18:2685–2700.
57. Willox I, Mirkina I, Westwick J, et al. Evidence for PI3K-dependent CXCR3 agonist-induced degranulation of human cord blood-derived mast cells. *Mol Immunol* 2010;47:2367–2377.
58. Xu T, Xu L, Meng P, et al. Angptl7 promotes insulin resistance and type 2 diabetes mellitus by multiple mechanisms including SOCS3-mediated IRS1 degradation. *FASEB J* 2020;34:13548–13560.
59. Banini BA, Sanyal AJ. NAFLD-related HCC. *Adv Cancer Res* 2021;149:143–169.
60. Peiseler M, Tacke F. Inflammatory mechanisms underlying nonalcoholic steatohepatitis and the transition to hepatocellular carcinoma. *Cancers (Basel)* 2021;13.
61. Karin M. New insights into the pathogenesis and treatment of non-viral hepatocellular carcinoma: a balancing act between immunosuppression and immunosurveillance. *Precis Clin Med* 2018;1:21–28.
62. Gleissner CA, Shaked I, Little KM, et al. CXC chemokine ligand 4 induces a unique transcriptome in monocyte-derived macrophages. *J Immunol* 2010;184:4810–4818.
63. Ruytinx P, Proost P, Van Damme J, et al. Chemokine-induced macrophage polarization in inflammatory conditions. *Front Immunol* 2018;9:1930.
64. Ruytinx P, Proost P, Struyf S. CXCL4 and CXCL4L1 in cancer. *Cytokine* 2018;109:65–71.
65. Mehlem A, Hagberg CE, Muhl L, et al. Imaging of neutral lipids by oil red O for analyzing the metabolic status in health and disease. *Nat Protoc* 2013;8:1149–1154.
66. Junqueira LC, Bignolas G, Brentani RR. Picrosirius staining plus polarization microscopy, a specific method for collagen detection in tissue sections. *Histochem J* 1979;11:447–455.
67. Ran FA, Hsu PD, Wright J, et al. Genome engineering using the CRISPR-Cas9 system. *Nat Protoc* 2013;8:2281–2308.
68. Charni-Natan M, Goldstein I. Protocol for primary mouse hepatocyte isolation. *STAR Protoc* 2020;1:100086.
69. Chen S, Zhou Y, Chen Y, et al. fastp: an ultra-fast all-in-one FASTQ preprocessor. *Bioinformatics* 2018;34:i884–i890.
70. Patro R, Duggal G, Love MI, et al. Salmon provides fast and bias-aware quantification of transcript expression. *Nat Methods* 2017;14:417–419.

71. Love MI, Huber W, Anders S. Moderated estimation of fold change and dispersion for RNA-seq data with DESeq2. *Genome Biol* 2014;15:550.
72. Dobin A, Davis CA, Schlesinger F, et al. STAR: ultrafast universal RNA-seq aligner. *Bioinformatics* 2013; 29:15–21.
73. Gao J, Aksoy BA, Dogrusoz U, et al. Integrative analysis of complex cancer genomics and clinical profiles using the cBioPortal. *Sci Signal* 2013;6:p11.
74. Ritchie ME, Phipson B, Wu D, et al. limma powers differential expression analyses for RNA-sequencing and microarray studies. *Nucleic Acids Res* 2015; 43:e47.
75. Steen CB, Liu CL, Alizadeh AA, et al. Profiling cell type abundance and expression in bulk tissues with CIBER-SORTx. *Methods Mol Biol* 2020;2117:135–157.
76. Chen Z, Huang A, Sun J, et al. Inference of immune cell composition on the expression profiles of mouse tissue. *Sci Rep* 2017;7:40508.

study, Dr Feiye Liu for her initial effort in creating *Ncoa5* floxed mice, and Dr Ying Qin for consultation on mouse liver histology.

CRediT Authorship Contributions

Yueqi Zhang (Conceptualization: Supporting; Data curation: Lead; Formal analysis: Lead; Investigation: Lead; Methodology: Lead; Resources: Lead; Software: Lead; Validation: Lead; Visualization: Lead; Writing – original draft: Lead; Writing – review & editing: Lead)

Yue Luo (Conceptualization: Supporting; Data curation: Supporting; Formal analysis: Supporting; Investigation: Supporting; Methodology: Supporting; Validation: Supporting; Visualization: Supporting; Writing – review & editing: Supporting)

Xinhui Liu (Conceptualization: Supporting; Data curation: Supporting; Formal analysis: Supporting; Investigation: Supporting; Methodology: Supporting; Validation: Supporting; Writing – review & editing: Supporting)

Matti Kiupel (Formal analysis: Supporting; Methodology: Supporting; Validation: Supporting; Visualization: Supporting; Writing – review & editing: Supporting)

Aimin Li (Funding acquisition: Supporting; Supervision: Supporting; Writing – review & editing: Supporting)

Hongbing Wang (Conceptualization: Supporting; Resources: Supporting; Writing – review & editing: Supporting)

Qing-Sheng Mi (Conceptualization: Supporting; Resources: Supporting; Writing – review & editing: Supporting)

Hua Xiao (Conceptualization: Lead; Data curation: Supporting; Formal analysis: Supporting; Funding acquisition: Lead; Investigation: Lead; Methodology: Lead; Project administration: Lead; Resources: Lead; Software: Lead; Supervision: Lead; Validation: Supporting; Visualization: Supporting; Writing – original draft: Lead; Writing – review & editing: Lead)

Received July 20, 2022. Accepted September 13, 2023.

Correspondence

Address correspondence to: Hua Xiao, MD, PhD, Department of Physiology, Michigan State University, 3193 Biomedical and Physical Sciences Building, East Lansing, Michigan 48824-3320. e-mail: xiaoh@msu.edu.

Acknowledgments

The authors thank Dr Myriam Aouadi for providing us with glucan shells and technical advice for this study. The authors thank Drs Huirong Xie and Elena Demireva at the Transgenic and Genome Editing Facility of MSU for using the CRISPR/Cas9 method to generate *Ncoa5* floxed mice used in our pilot

Conflicts of interest

The authors disclose no conflicts.

Funding

Supported by the National Cancer Institute grant (R01 CA188305) and the Discretionary Funding Initiative grants of Michigan State University (GR101538 and GR100453) to H. X., Henry Ford Hospital and Michigan State University cancer grant to H.X and Q-S. M. Y.Z. was partially supported by the Aitch Fellowship of the Aitch Foundation and a dissertation completion fellowship of the Graduate School of Michigan State University. Y.L. and X.L. were partially supported by a fellowship from the Integrated Hospital of Traditional Chinese Medicine, Southern Medical University.